This article has been accepted for publication in IEEE Transactions on Communications. This is the author's version which has not been fully edited and content may change prior to final publication. Citation information: DOI 10.1109/TCOMM.2023.3250454

Enhanced Secure Communication via Novel Double-Faced Active RIS

Yuan Guo, Yang Liu, Qingqing Wu, Qingjiang Shi, and Yang Zhao

Abstract—**Although the reconfigurable intelligent surface (RIS) technology is envisioned promising to enhance communication from all aspects, including physical-layer security, increasing concerns have lately been cast onto its defects—the severe "double-fading" loss and its confined-to-half-space coverage. Diverse novel RIS architectures have recently emerged to partially overcome these shortcomings, yet perfect solution is still absent. This paper proposes a novel double-faced active (DFA)-RIS structure to surmount the above two prominent defects simultaneously. Furthermore, we utilize the DFA-RIS to promote secrecy performance via jointly designing access point (AP)'s beamforming and DFA-RIS configuration towards maximizing sum secrecy rate (SR). The optimization problem is highly challenging due to the constraints deriving from the DFA-RIS architecture, especially the presence of power splitting parameters. By leveraging majorization–minimization (MM) and penalty dual decomposition (PDD) methods, we develop an efficient solution that updates all variables via convex optimization techniques. Our proposed solution is significant and general as it is applicable to all other cutting-the-edge RIS architectures to maximize sum SR, which has not yet been thoroughly worked out. Numerical results verify the convergence and effectiveness of our proposed algorithm and demonstrate that our proposed DFA-RIS architecture outperforms all other state-of-the-art RIS techniques to enhance communication security.**

Index Terms—**reconfigurable intelligent surface (RIS), physical layer security, majorization-minimization (MM) algorithm, penalty dual decomposition (PDD) method.**

I. Introduction

Recently, the rising technology of reconfigurable intelligent surface (RIS) [1], which is also widely known as intelligent reflecting surface (IRS) [2], has been cast with great attentions from both academia and industry and is envisioned as a potential solution for the next generation communication system. The RIS can empower communication networks with additional beamforming capability via reflecting and adjusting phase shifts of the incoming signals at a relatively low energy and hardware cost. These advantages make RIS highly promising. Its potentials in boosting communication performance in various respects, including spectral efficiency, power consumption, energy efficiency and so on, have been extensively corroborated by the recent researches, e.g., see [1]−[3] and the reference therein.

At the same time, along with studies on RIS going deeper, some intrinsic shortcomings of the classical passive RIS have recently been unveiled by a number of latest researches [4]−[10]. Specifically, the single-faced passive RIS suffers from two prominent drawbacks: i) the signal reflected by RIS experiences severe attenuation due to the multiplicative nature of the fading loss of the cascaded channels [4]−[7], which is named as "double fading" effect in [5], ii) conventional RIS can only serve mobile users within half-space.

To overcome the aforementioned shortcomings, diverse novel RIS architectures have emerged very recently. Specifically, to combat the curse of double fading, a type of *active*-RIS structure has been proposed in [6]−[9] lately, i.e., active reflecting-only RIS [6]−[8] and active refracting-only RIS [9]. The active-RIS introduces amplifiers into the conventional reflecting elements and hence can magnify the signals when it "reflects/refracts" the impinging electromagnetic (EM) waves. As demonstrated by the experiment results in [6] and [7], the active architecture can significantly improve the RIS coverage and system's spectral efficiency. Besides, to extend the coverage of the classical RIS from half-space to full-space, a type of *simultaneously reflective and refractive* RIS structure has also been put forward recently. For instance, a type of intelligent omni-surface (IOS) has been proposed in [10]. The elements of IOS can realize reflecting one part of the incoming EM waves while at the same time allowing the other part penetrating the surface and propagating into the backside space. Similar functionality has also been implemented by the simultaneously transmitting and reflecting RIS (STAR-RIS) proposed in [11] using different hardware techniques.

A. Related Works

As mentioned before, a rich body of literature has demonstrated the deployment of RIS could improve the communication system's performance. Among them, one important fact was to promote the physical layer security via RIS techniques [12]−[25]. For instance, the authors in [12] investigated the secrecy rate (SR) maximization problem in an RIS-aided multiple-input single-output (MISO) system with one legitimate information receiver (IR) and one eavesdropper (EV).

The work of Yang Liu is supported in part by Grant No. DUT20RC(3)029 and the Open Research Project Programme of the State Key Laboratory of Internet of Things for Smart City (University of Macau) (Ref. No.: SKLIoTSC(UM)-2021-2023/ORP/GA01/2022). The work of Q. Shi was supported in part by the National Key Research and Development Project under grant 2017YFE0119300, and in part by the NSFC under grants 61671411, 61731018, 62231019 and U1709219.

Yang Liu is the corresponding author.

Y. Guo and Y. Liu are with the School of Information and Communication Engineering, Dalian University of Technology, Dalian, China, email: yuanguo@mail.dlut.edu.cn, yangliu_613@dlut.edu.cn.

Q. Wu is with the Department of Electronic Engineering, Shanghai Jiao Tong University, Shanghai, China, email: qingqingwu@sjtu.edu.cn.

Q. Shi is with the School of Software Engineering, Tongji University, Shanghai, China, and also with the Shenzhen Research Institute of Big Data, Shenzhen, China, email: shiqj@tongji.edu.cn.

Y. Zhao is with Singapore Institute of Manufacturing Technology, A*STAR, Singapore, email: zhao_yang@simtech.a-star.edu.sg.

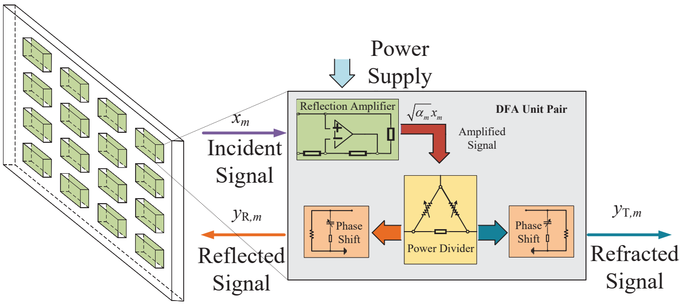

Fig. 1. Architecture of the DFA-RIS element.

The paper [13] considered maximizing the sum SR of multiple valid IRs, with each IR being wiretapped by one specific EV. Besides, the works [14] and [15] considered the sum-rate maximization while constraining the information rate leaking to potential EVs. The paper [16] considered to maximize the covert rate of user in RIS-assisted non-orthogonal multiple access (NOMA) system. The recent work [17] was the first one to deploy active-type RIS to enhance communication security. In [17], a communication system with one IR and one EV was considered and numerical results demonstrated that the deployment of active-RIS could significantly improve the security. The paper [18] considered power minimization in the downlink MISO system assisted by active-RIS, which consist of one IR and one EV. The literature [19] studied power minimization using active-RIS while assuring that the signal-to-interference-plus-noise-ratio (SINR) requirements for the IRs and EVs were satisfied, respectively. The authors of [20] aimed to improve the secrecy performance in the passive RIS aided internet-of-things (IoT) network by leveraging active refracting-type RIS-based transmitter. The paper [21] was the first to study using STAR-RIS to improve communication security, where one IR and one EV were located on each side the RIS, respectively. The work [22] studied sum SR maximization in a STAR-RIS aided communication network consisting of one EV. The authors of [23] considered a max-min SR problem in an STAR-RIS aided MISO system consisting of multiple IRs and EVs. The works [24] and [25] considered maximizing the secrecy energy efficiency in STAR-RIS aided secure NOMA system and IOS aided secure unmanned aerial vehicle (UAV) communication system, respectively.

B. Motivations and Contributions

At this point, existing researches on RIS-assisted secure communication are either based on pure passive RIS devices, e.g., [12]−[16], or single-faced active-RIS device, e.g., [17]−[20]. As unveiled by the recent works [7], [8], pure passive RIS suffers from the double-fading effect that severely weakens its beamforming gain. At the same time, as reflected by the studies [10], [11], extending the coverage of RIS from half-space to full-space can benefit all mobile users located at any positions.

Moreover, the sum SR problem with multiple EVs has not been thoroughly settled by the existing literature, i.e., [12]−[15], [17], [20], [21] and [22]. Since the sum SR problem is difficult, to circumvent this difficulty, all existing literature makes concessions to simplify problems. For instance, the papers [14] and [15] imposed constraints on EVs receiving information rate, which indeed allowed information leakage. Other papers just assumed that there existed only one EV in the system [12], [17], [21] and [22], or any IR would only be wiretapped by one specific EV, e.g., [13] and [20]. These assumptions have indeed undermined the generality of their model.

Inspired by the above inspections, we are motivated to enhance the communication security via RIS devices which can simultaneously amplify incoming EM waves and cover all mobile users in any directions. Towards this end, this paper proposes a novel double-faced active (DFA)-RIS architecture, which possesses the advantages of both active-RIS [7] and IOS [10], and can be leveraged to further enhance physical-layer security of wireless system consisting of multiple IRs and EVs. Specifically, the main contributions of this paper are elaborated as follows.

- Firstly, this paper proposes a novel DFA-RIS architecture, as shown in Fig. 1. This new design can i) effectively combat the severe double-fading loss suffered by the pure passive RIS, e.g., the conventional RIS [1] and the IOS [10]; ii) extend the coverage from half-space [1], [7] to full-space; iii) be implemented by realistic techniques using low-cost basic analog components (as will be discussed later in Sec. II.A).
- Secondly, we employ the proposed DFA-RIS to enhance the SR of a communication system via jointly optimizing the AP's beamforming and DFA-RIS' configuration. Compared to the existing literature on RIS-aided secure communication [12]−[25], our considered sum SR optimization is based on the most generic setting consisting of multiple EVs and our DFA-RIS architecture subsumes the conventional passive RIS [12]−[16], the active-RIS in [17]−[20], and the IOS/STAR-RIS in [21]−[25] as special cases and therefore our study provides a unified solution to SR maximization (as will be explained in Sec. III.C).
- The joint AP's beamforming and DFA-RIS configuration design to improve SR is a highly non-convex problem due to the presence of the power splitting coefficients and constant-modulus constraints for phase-shifters. Via combining mean-inequality based majorization-minimization (MM) transformation and the penalty dual decomposition (PDD) method, we successfully develop an iterative solution that updates the power splitting coefficients and phase-shifters via convex optimization techniques.
- Extensive numerical results are provided to verify the convergence and efficiency of our proposed algorithms, and validate the advantages of the proposed DFA-RIS architecture over other emerging RIS structures, e.g., active-RIS [6]−[8] and IOS/STAR-RIS [10], [11]. Besides, compared with the passive type RIS, the DFA-RIS with the proposed algorithm requires only about 40% power consumption to achieve the approximate level of sum SR performance.

The rest of the paper is organized as follows. Section II will discuss the DFA-RIS' architecture, implementation and its associated signal model. Section III will introduce the model of a secure communication system assisted by DFA-RIS and formulate the joint secure beamforming design problem. Section IV and Section V will elaborate the algorithm development and present numerical results, respectively. Section VI will conclude the paper.

II. DFA-RIS' Architecture

This section will elaborate the novel DFA-RIS architecture, including its practical implementation and signal model.

A. DFA-RIS' Architecture and Implementation

The DFA-RIS architecture deploys element arrays on both sides of a plate with their elements being aligned, as shown in Fig. 1. Each pair of aligned elements on the opposite faces are connected by circuits embedded within the plate. Similar to the single-faced active-RIS structure proposed in [7] and [8], the incident signal is first enlarged by a reflection amplifier (RA). Then, the output of the RA is divided into two parts by a tunable power dividing unit (PDU) and both parts are fed into the pair of the opposite phase shifters. Therefore, our proposed DFA-RIS architecture can realize reflecting and transmitting the incoming signals simultaneously, just as the STAR-RIS raised in [11], and adjust both the amplitudes and phase-shifts of the outgoing signals.

It should be pointed out that the DFA-RIS architecture proposed above is indeed realistic and can be implemented via existing technologies. As previously discussed, the DFA-RIS unit is composed of three key components: i) RA, ii) tunable PDU and iii) phase-shifters. Besides the commonly used phase-shifters, the RA and the tunable PDU can both be implemented via basic analog devices.

For the RA, it is in principle an active-load amplifier with negative equivalent input resistance input resistance and can be implemented with various analog circuits. For instance, the authors of [26] implement a novel RA by utilizing aperture-coupled microstrip path and use it to construct a 48-element reconfigurable reflect-array that can amplify impinging EM waves. The authors of [27] and [28] exploit field effect transistors (FETs) and tunnel diodes, respectively, to realize novel RAs and use them to build retrodirective antenna arrays having beam steering capabilities. The authors of [29] and [30] adopt complementary metal oxide semiconductor (CMOS) techniques to implement RA and employ it to construct full-duplex active reconfigurable reflect-array. Note that the RA is also exploited in the emerging singled-faced active-RIS design in [7] and [8].

Besides the RA, tunable PDUs can also be realized via low-cost analog components nowadays. In fact, the last decade has witnessed great progress in PDU technology development. Via combining adjustable varactors/diodes with the conventional power dividers or couplers, we are now able to implement PDUs with tunable power dividing ratio (PDR) (PDR means the power ratio between the two outputs of the PDU). Especially, tunable PDUs with extremely-wide-range PDR have become reality within the last five years. For example, via concatenating two couplers and phase-shifters, the authors of [31] propose a novel PDR structure whose tunable PDR varies from -25dB to 25dB. Based on the reconfigurable synthesize transmission line (RSTL) techniques, the works [32] and [33] develop PDUs having wide PDR range of -25dB $\sim$ 25dB and -39dB $\sim$ 29dB, respectively. Another novel Π-type reconfigurable coupler has recently been proposed in [34], whose controllable PDR ranges from -20.5dB to 21.3dB. It is worth noting that tunable PDU has already been utilized in various applications. For instance, the tunable PDU is employed in simultaneous wireless information and power transfer (SWIPT) device in [35], where the incoming signal is divided into two parts with a configurable ratio and fed into information and energy receivers. In [36], a novel 2-way tunable power divider is employed in wearable multiple-input-multiple-output (MIMO) antenna to enhance its beamforming capability.

Besides, the authors of [37] designed an active sub-array RIS architecture via combining power amplifier (PA), power divider with fixed PDR and phase shifter, which can achieve a gain form 7.7dB to 12.2dB operating at 5.0GHz to 6.0GHz. The work [7] implemented active RIS operating at 2.36GHz band by combining RA and phase shifter. The authors of [29] leveraged thr RA and phase shifter to construct a full-duplex active reconfigurable reflect-array in [30], which had strong beamforming capability. By concatenating tunable PDU and phase shifter, the authors in [38] designed an antenna array's radio-frequency (RF) frontend operating at 1GHz, to empower the transmitter with beamsteering capability.

The above discussions indicate that our proposed DFA-RIS can be implemented by existing analog circuit techniques.

B. Signal Model

Based on the above architecture, we establish the signal model of the DFA-RIS. Assume that $x_{R,m}$ is the incident signal onto the m-th element of the DFA-RIS. The reflected and refracted signal can be respectively modeled as

$$y_{R,m} = \phi_{R,m}\varsigma_m\sqrt{\alpha_m}(x_{R,m}+v_m), \quad (1)$$

$$y_{T,m} = \phi_{T,m}\sqrt{1-\varsigma_m^2}\sqrt{\alpha_m}(x_{R,m}+v_m), \quad (2)$$

where $\sqrt{\alpha_m}$ is the amplifying coefficient, $\varsigma_m \in [0,1]$ is the power-splitting parameter adjusting the PDR, and $\phi_{R,m} = e^{j\theta_{R,m}}$ and $\phi_{T,m} = e^{j\theta_{T,m}}$ denote the phase shifts of the reflected and refracted signal, respectively, and v_m is the introduced noise at the active RIS, $\forall m \in \mathcal{M} \triangleq \{1,\ldots,M\}$ with M denoting the total number of DFA-RIS elements. Therefore, the reflected and refracted signals by the DFA-RIS can be expressed as

$$\mathbf{y}_R = \mathbf{\Phi}_R\mathbf{E}_R\mathbf{A}(\mathbf{x}_R+\mathbf{v}),\ \mathbf{y}_T = \mathbf{\Phi}_T\mathbf{E}_T\mathbf{A}(\mathbf{x}_R+\mathbf{v}), \quad (3)$$

respectively, where $\mathbf{x}$ is the incident signal, $\mathbf{v}$ denotes the introduced noise vector with $\mathbf{v} \backsim \mathcal{CN}(0,\sigma_v^2\mathbf{I}_M)$, $\mathbf{A} \triangleq \mathrm{Diag}(\sqrt{\boldsymbol{\alpha}})$ and $\boldsymbol{\alpha} \triangleq [\alpha_1,\ldots,\alpha_M]^T$ represent the amplifying coefficients, $\mathbf{E}_R \triangleq \mathrm{Diag}([\varsigma_1,\ldots,\varsigma_M])$ and $\mathbf{E}_T \triangleq \mathrm{Diag}([\sqrt{1-\varsigma_1^2},\ldots,\sqrt{1-\varsigma_M^2}])$ denote power splitting parameters, respectively, and $\boldsymbol{\phi_R} \triangleq [e^{j\theta_{R,1}},\ldots,e^{j\theta_{R,M}}]$ and $\boldsymbol{\phi_T} \triangleq [e^{j\theta_{T,1}},\ldots,e^{j\theta_{T,M}}]$ represent the phase shifts of the

This article has been accepted for publication in IEEE Transactions on Communications. This is the author's version which has not been fully edited and content may change prior to final publication. Citation information: DOI 10.1109/TCOMM.2023.3250454

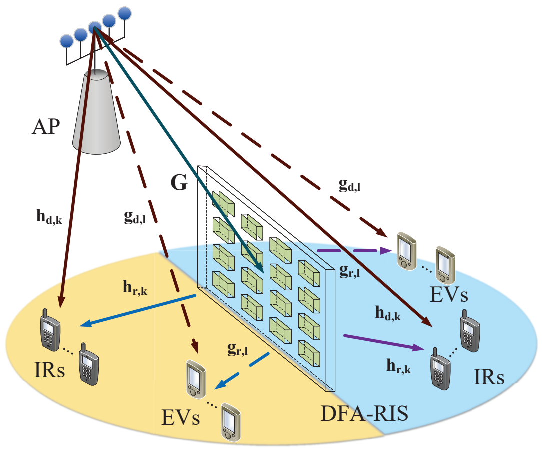

Fig. 2. A DFA-RIS assisted secure communication system.

reflected and refracted signals, respectively, with $\Phi_R \triangleq \mathrm{Diag}(\boldsymbol{\phi_R})$ and $\Phi_T \triangleq \mathrm{Diag}(\boldsymbol{\phi_T})$.

Considering the fact that a low-cost amplifier has limited magnifying capability, there should be a power limit for each amplifier, which is given by

$$\mathbb{E}\{\alpha_m|x_{R,m}+v_m|^2\} \leq P_m, \forall m \in \mathcal{M}, \quad (4)$$

where P_m is the effective transmit radio power (TRP) limit.

Besides, the overall transmit power of the DFA-RIS is limited by its power supply, which leads to

$$\mathbb{E}\{\|\mathbf{y}_R\|_2^2+\|\mathbf{y}_T\|_2^2\} = \mathbb{E}\{\|\mathbf{A}(\mathbf{x}_R+\mathbf{v})\|_2^2\} \leq P_r, \quad (5)$$

with P_r being the total effective TRP of the RIS.

III. System Model and Problem Formulation

In this section, we will elaborate the system model of a DFA-RIS assisted network and the associated secure beamforming design problem.

A. System Model

As shown in Fig. 2, we consider a MISO downlink secure wireless communication system that comprises one access point (AP), one DFA-RIS, K IRs and L EVs, with $\mathcal{K} \triangleq \{1,\ldots,K\}$ and $\mathcal{L} \triangleq \{1,\ldots,L\}$. Assisted by the DFA-RIS, the AP equipped with N antennas communicates with the single-antenna IRs. At the same time, the single-antenna EVs potentially decode signals transmitted to IRs. The DFA-RIS divides the entire three-dimensional (3D) space into two halves.

We name the IRs/EVs lying within the same half space together with AP as *reflective* IRs/EVs and denote them as $\mathcal{K}_R \triangleq \{1,\ldots,K_R\}$ and $\mathcal{L}_R \triangleq \{1,\ldots,L_R\}$, respectively. Similarly, the IRs/EVs in the other half space are named as *refractive* IRs/EVs and denoted as $\mathcal{K}_T \triangleq \{K_R+1,\ldots,K\}$ and $\mathcal{L}_T \triangleq \{L_R+1,\ldots,L\}$, respectively.

The transmit signal of the AP can be expressed as

$$\mathbf{x} = \sum\nolimits_{k=1}^{K} \mathbf{f}_k s_k. \quad (6)$$

where $\mathbf{f}_k \in \mathbb{C}^{N\times 1}$ and s_k denote the transmit beamformer and the information symbol for the k-th IR, respectively. We assume the information symbols $\{s_k\}$ are mutually uncorrelated and each has zero mean and unit variance.

The received signals at the k-th IR and l-th EV can be written as

$$y_{B,k} = \mathbf{h}_{d,k}^H\mathbf{x} + \mathbf{h}_{r,k}^H\boldsymbol{\Phi}_{\imath(k)}\mathbf{E}_{\imath(k)}\mathbf{A}\mathbf{G}\mathbf{x} + \mathbf{h}_{r,k}^H\boldsymbol{\Phi}_{\imath(k)}\mathbf{E}_{\imath(k)}\mathbf{A}\mathbf{v} + n_{B,k},\ \forall k, \quad (7)$$

$$y_{E,l} = \mathbf{g}_{d,l}^H\mathbf{x} + \mathbf{g}_{r,l}^H\boldsymbol{\Phi}_{\imath(l)}\mathbf{E}_{\imath(l)}\mathbf{A}\mathbf{G}\mathbf{x} + \mathbf{g}_{r,l}^H\boldsymbol{\Phi}_{\imath(l)}\mathbf{E}_{\imath(l)}\mathbf{A}\mathbf{v} + n_{E,l},\ \forall l, \quad (8)$$

respectively, where $\mathbf{G} \in \mathbb{C}^{M\times N}$, $\mathbf{h}_{d,k} \in \mathbb{C}^{N\times 1}$, $\mathbf{g}_{d,l} \in \mathbb{C}^{N\times 1}$, $\mathbf{h}_{r,k} \in \mathbb{C}^{M\times 1}$, and $\mathbf{g}_{r,l} \in \mathbb{C}^{M\times 1}$ represent channels associated with the links of AP-RIS, AP-IR$_k$, AP-EV$_l$, RIS-IR$_k$ and RIS-EV$_l$, respectively. Besides, we denote $n_{B,k} \sim \mathcal{CN}(0,\sigma_{B,k}^2)$ and $n_{E,l} \sim \mathcal{CN}(0,\sigma_{E,l}^2)$ as the noise at IR$_k$ and EV$_l$, respectively. Taking similar considerations as in [12], [13], [17]−[21], we assume that CSI are known at the AP. [1]

To simplify notations, we introduce the category mapping $\imath(k) : \mathcal{K} \to \{R,T\}$, such that $\imath(k) = R$ if $k \in \mathcal{K}_R$ and $\imath(k) = T$ if $k \in \mathcal{K}_T$. Note that the wireless link $\mathbf{h}_{r,k}$ originates from exactly one of the two opposite faces of the DFA-RIS, according to the category $\imath(k)$ of IR$_k$. The above category mapping also applies to any EV $l \in \mathcal{L}$.

By defining $\mathbf{G} \triangleq [\bar{\mathbf{g}}_1,\ldots,\bar{\mathbf{g}}_M]^T$ with $\bar{\mathbf{g}}_m^T$ being the m-th row of $\mathbf{G}$, the DFA-RIS' element-wise power constraint can be explicitly written as

$$\alpha_m \sum\nolimits_{k=1}^{K} |\bar{\mathbf{g}}_m^T\mathbf{f}_k|^2 + \alpha_m\sigma_v^2 \leq P_m,\ \forall m \in \mathcal{M}, \quad (9)$$

and the total power constraint of DFA-RIS is given as

$$\sum\nolimits_{k=1}^{K} \|\mathbf{A}\mathbf{G}\mathbf{f}_k\|_2^2 + \sigma_v^2\|\mathbf{A}\|_F^2 \leq P_r. \quad (10)$$

The SINR of the IR$_k$ can be expressed as

$$\gamma_k^B = \frac{|\mathbf{h}_k^H\mathbf{f}_k|^2}{\sum_{j\neq k}^{K}|\mathbf{h}_k^H\mathbf{f}_j|^2 + \sigma_v^2\|\mathbf{A}\mathbf{E}_{\imath(k)}\mathbf{h}_{r,k}\|_2^2 + \sigma_{B,k}^2},\ \forall k, \quad (11)$$

where $\mathbf{h}_k^H \triangleq \mathbf{h}_{d,k}^H + \mathbf{h}_{r,k}^H\boldsymbol{\Phi}_{\imath(k)}\mathbf{E}_{\imath(k)}\mathbf{A}\mathbf{G}$ and $\|\boldsymbol{\Phi}_{\imath(k)}^*\mathbf{A}\mathbf{E}_{\imath(k)}\mathbf{h}_{r,k}\|_2^2 = \|\mathbf{A}\mathbf{E}_{\imath(k)}\mathbf{h}_{r,k}\|_2^2$.

The receiving SINR at EV$_l$ for decoding symbol s_k can be given by

$$\gamma_{k,l}^E = \frac{|\mathbf{g}_l^H\mathbf{f}_k|^2}{\sum_{j\neq k}^{K}|\mathbf{g}_l^H\mathbf{f}_j|^2 + \sigma_v^2\|\mathbf{A}\mathbf{E}_{\imath(l)}\mathbf{g}_{r,l}\|_2^2 + \sigma_{E,l}^2},\ \forall k,\ \forall l, \quad (12)$$

where $\mathbf{g}_l^H \triangleq \mathbf{g}_{d,l}^H + \mathbf{g}_{r,l}^H\boldsymbol{\Phi}_{\imath(l)}\mathbf{E}_{\imath(l)}\mathbf{A}\mathbf{G}$ and $\|\boldsymbol{\Phi}_{\imath(l)}^*\mathbf{A}\mathbf{E}_{\imath(l)}\mathbf{g}_{r,l}\|_2^2 = \|\mathbf{A}\mathbf{E}_{\imath(l)}\mathbf{g}_{r,l}\|_2^2$.

Therefore, according to [39], the achievable SR at k-th IR is defined as

$$R_{SR_k} \triangleq \left[\log(1+\gamma_k^B) - \max_{\forall l\in\mathcal{L}} \log(1+\gamma_{k,l}^E)\right]^+,\ \forall k, \quad (13)$$

where $[x]^+ \triangleq \max\{x,0\}$. Since the optimal SR is usually the non-negative, we omit the operator $[\,]^+$ in the rest of this paper [40].

B. Problem Formulation

Our goal is to maximize the sum SR of all IRs via jointly optimizing the transmit beamformers $\{\mathbf{f}_k\}$, the reflected and refracted phase shifts $\boldsymbol{\phi}_R$ and $\boldsymbol{\phi}_T$, the amplifying coefficients $\mathbf{A}$ and the power splitting coefficients $\boldsymbol{\varsigma}$. The optimization problem is formulated as

$$(\mathrm{P0}):\ \max_{\{\mathbf{f}_k\},\boldsymbol{\alpha},\boldsymbol{\varsigma},\boldsymbol{\phi}_R,\boldsymbol{\phi}_T}\ \sum\nolimits_{k=1}^{K} R_{SR_k} \quad (14a)$$

[1] In fact, the solution developed in this paper can be easily extended to robust beamforming design when CSI is not perfect [24]. Due to space of limit, we leave the imperfect CSI case for future study.

$$\text{s.t.} \sum_{k=1}^{K} \|\mathbf{f}_k\|_2^2 \leq P_{AP}, \tag{14b}$$

$$\sum_{k=1}^{K} \|\mathbf{A}\mathbf{G}\mathbf{f}_k\|_2^2 + \sigma_v^2 \|\mathbf{A}\|_F^2 \leq P_r, \tag{14c}$$

$$\alpha_m \sum_{k=1}^{K} |\bar{\mathbf{g}}_m^T \mathbf{f}_k|^2 + \alpha_m \sigma_v^2 \leq P_m, \ \forall m, \tag{14d}$$

$$\varsigma_m \in [0,1], \ \forall m, \tag{14e}$$

$$\boldsymbol{\alpha} \geq \mathbf{0}, \tag{14f}$$

$$|\phi_{R,m}| = 1, |\phi_{T,m}| = 1, \ \forall m, \tag{14g}$$

where P_{AP} is the maximum transmission power of the AP. The problem (P0) is difficult due to its highly non-convex objective and constraints.

C. Connections with Other Emerging RIS Techniques

It is worth noting that the secure beamforming design problem (P0) considering the DFA-RIS is closely related to those employing other cutting-the-edge RIS architectures, as elaborated below.

i) Connection with the passive RIS

By setting $\boldsymbol{\alpha} = \mathbf{1}$, $\boldsymbol{\varsigma} = \mathbf{1}$, $\sigma_v = 0$, $P_r = \infty$, $\{P_m = \infty\}$, $\mathcal{K} = \mathcal{K}_R$ and $\mathcal{L} = \mathcal{L}_R$, the problem (P0) reduces to the SR maximization using the classical passive RIS [1], [2].

ii) Connection with the active-RIS

By setting $\boldsymbol{\varsigma} = \mathbf{1}$, $\mathcal{K} = \mathcal{K}_R$ and $\mathcal{L} = \mathcal{L}_R$ (alternatively, by setting $\boldsymbol{\varsigma} = \mathbf{0}$, $\mathcal{K} = \mathcal{K}_T$ and $\mathcal{L} = \mathcal{L}_T$), the problem (P0) reduces to SR maximization using the single-faced active RIS proposed in [7] and [8].

ii) Connection with the IOS/STAR-RIS

By setting $\boldsymbol{\alpha} = \mathbf{1}$, $\sigma_v = 0$, $P_r = \infty$ and $\{P_m = \infty\}$, the problem (P0) reduces to SR maximization using IOS or STAR-RIS proposed in [10] and [11] (with the amplifier power constraints (14d) omitted).

As discussed above, via appropriately fixing parts of the variables, the SR maximization using all other RIS structures [12]−[25] can all be considered as simplified special cases of our considered problem (P0). Therefore, the secure beamforming design in this paper can be regarded as a unifying solution for all the above state-of-the-art RIS architectures.

IV. Algorithm Design

A. Problem Reformulation

To make the above problem (P0) more tractable, we first transform its objective via invoking the following lemma [41].

Lemma 1. *Define a $T \times T$ matrix function*

$$\mathbf{E}(\mathbf{U},\mathbf{V}) \triangleq (\mathbf{I} - \mathbf{U}^H\mathbf{H}\mathbf{V})(\mathbf{I} - \mathbf{U}^H\mathbf{H}\mathbf{V})^H + \mathbf{U}^H\mathbf{N}\mathbf{U}, \tag{15}$$

where $\mathbf{N}$ is any positive definite matrix. The following three facts hold true [41].

Fact-1 For any positive definite matrix $\mathbf{E} \in \mathbb{C}^{T\times T}$,

$$-\text{logdet}(\mathbf{E}) = \max_{\mathbf{W}\succ\mathbf{0}} \text{logdet}(\mathbf{W}) - \text{Tr}(\mathbf{W}\mathbf{E}) + T. \tag{16}$$

In fact, the maximization problem on the right hand of (16) is concave with respect to (w.r.t.) $\mathbf{W}$ and therefore its optimal solution can be easily obtained via setting its derivative to zero, which yields $\mathbf{W}^\star = \mathbf{E}^{-1}$ and hence (16) can be verified.

Fact-2 For any positive definite matrix $\mathbf{W}$,

$$\mathbf{U}^\star \triangleq \arg\min_{\mathbf{U}} \text{Tr}(\mathbf{W}\mathbf{E}(\mathbf{U},\mathbf{V})) = (\mathbf{N} + \mathbf{H}\mathbf{V}\mathbf{V}^H\mathbf{H}^H)^{-1}\mathbf{H}\mathbf{V}. \tag{17}$$

The minimization problem in (17) is indeed a non-constrained convex quadratic problem w.r.t. $\mathbf{U}$ and therefore its optimal value could be obtained via checking its first order optimality condition (setting derivation to zero).

Besides, by substituting (17) into (15), we can obtain

$$\mathbf{E}(\mathbf{U}^\star,\mathbf{V}) = (\mathbf{I} + \mathbf{V}^H\mathbf{H}^H\mathbf{N}^{-1}\mathbf{H}\mathbf{V})^{-1}. \tag{18}$$

Fact-3 The following identity holds

$$\begin{aligned}&\text{logdet}(\mathbf{I} + \mathbf{H}\mathbf{V}\mathbf{V}^H\mathbf{H}^H\mathbf{N}^{-1}) \\ &= \max_{\mathbf{W}\succ\mathbf{0},\mathbf{U}} \text{logdet}(\mathbf{W}) - \text{Tr}(\mathbf{W}\mathbf{E}(\mathbf{U},\mathbf{V})) + T.\end{aligned} \tag{19}$$

Fact-3 stands via directly applying Fact-1 and Fact-2. Indeed, to solve the maximization problem on the right hand side of (19), we first invoke Fact-1 to eliminate $\mathbf{W}$ and then utilize Fact-2 to cancel $\mathbf{U}$ to reach the result on the left hand side of (19).

Firstly, we introduce the auxiliary variables $\boldsymbol{\omega}_B = [\omega_{B_1}, \ldots, \omega_{B_K}]^T$ and $\boldsymbol{\beta} = [\beta_1, \ldots, \beta_K]^T$, with each pair of ω_{B_k} and β_k corresponding to $\mathbf{W}$ and $\mathbf{U}$ in (19) and define the mean square error (MSE) function $e_k(\{\mathbf{f}_k\}, \boldsymbol{\alpha}, \boldsymbol{\varsigma}, \beta_k)$ as follows

$$\begin{aligned}&e_k(\{\mathbf{f}_k\}, \boldsymbol{\alpha}, \boldsymbol{\varsigma}, \beta_k) = (1 - \beta_k^* \mathbf{h}_k^H \mathbf{f}_k)(1 - \beta_k^* \mathbf{h}_k^H \mathbf{f}_k)^H \\ &+ |\beta_k|^2 \Big(\sum_{j\neq k}^{K} |\mathbf{h}_k^H \mathbf{f}_j|^2 + \sigma_v^2 \|\mathbf{A}\mathbf{E}_{\imath(k)}\mathbf{h}_{r,k}\|_2^2 + \sigma_{B,k}^2\Big),\end{aligned} \tag{20}$$

which corresponds to $\mathbf{E}$ in (16). By invoking *Fact-3* of Lemma 1, $\log(1+\gamma_k^B)$ can be equivalently written as (22), shown at the top of next page.

Next, we rewrite $\log(1+\gamma_{k,l}^E)$ as follows

$$\begin{aligned}&\log(1+\gamma_{k,l}^E) \\ &= \underbrace{\log\Big(1 + \big(\sum_{j=1}^{K} |\mathbf{g}_l^H \mathbf{f}_j|^2 + \sigma_v^2 \|\mathbf{A}\mathbf{E}_{\imath(l)}\mathbf{g}_{r,l}\|_2^2\big)\sigma_{E,l}^{-2}\Big)}_{f_{E1_{k,l}}} \\ &- \underbrace{\log\Big(1 + \big(\sum_{j\neq k}^{K} |\mathbf{g}_l^H \mathbf{f}_j|^2 + \sigma_v^2 \|\mathbf{A}\mathbf{E}_{\imath(l)}\mathbf{g}_{r,l}\|_2^2\big)\sigma_{E,l}^{-2}\Big)}_{f_{E2_{k,l}}},\end{aligned} \tag{21}$$

By introducing intermediate variables $\mathcal{C}^{K\times L} \ni \boldsymbol{\Omega}_E \triangleq [\omega_{E_{1,1}}, \ldots, \omega_{E_{1,L}}; \omega_{E_{2,1}}, \ldots, \omega_{E_{2,L}}; \ldots; \omega_{E_{K,1}}, \ldots, \omega_{E_{K,L}}]$, with each $\omega_{E_{k,l}}$ corresponding to the $\mathbf{W}$ in (16), the function $f_{E1_{k,l}}(\{\mathbf{f}_k\}, \boldsymbol{\alpha}, \boldsymbol{\varsigma}, \boldsymbol{\phi}_{\imath(l)})$ in (21) can be equivalently transformed into (23), shown at the top of next page.

Based on the above transformations, the problem (P0) can be equivalently written as

$$\begin{aligned}\text{(P1)}: &\max_{\substack{\{\mathbf{f}_k\},\boldsymbol{\alpha},\boldsymbol{\varsigma},\boldsymbol{\phi}_R,\\ \boldsymbol{\phi}_T,\boldsymbol{\omega}_B,\boldsymbol{\beta},\boldsymbol{\Omega}_E}} \sum_{k=1}^{K} \{f_{B_k}(\{\mathbf{f}_k\}, \boldsymbol{\alpha}, \boldsymbol{\varsigma}, \boldsymbol{\phi}_{\imath(k)}, \omega_{B_k}, \beta_k) \\ &- \max_{\forall l\in\mathcal{L}} \{\hat{f}_{E1_{k,l}}(\{\mathbf{f}_k\}, \boldsymbol{\alpha}, \boldsymbol{\varsigma}, \boldsymbol{\phi}_{\imath(l)}, \omega_{E_{k,l}}) - f_{E2_{k,l}}(\{\mathbf{f}_k\}, \boldsymbol{\alpha}, \boldsymbol{\varsigma}, \boldsymbol{\phi}_{\imath(l)})\}\}\end{aligned} \tag{24a}$$

s.t. (14b) − (14g),

with $f_{B_k}(\{\mathbf{f}_k\}, \boldsymbol{\alpha}, \boldsymbol{\varsigma}, \boldsymbol{\phi}_{\imath(k)}, \omega_{B_k}, \beta_k)$, $\hat{f}_{E1_{k,l}}(\{\mathbf{f}_k\}, \boldsymbol{\alpha}, \boldsymbol{\varsigma}, \boldsymbol{\phi}_{\imath(l)}, \omega_{E_{k,l}})$ and $f_{E2_{k,l}}(\{\mathbf{f}_k\}, \boldsymbol{\alpha}, \boldsymbol{\varsigma}, \boldsymbol{\phi}_{\imath(l)})$ being defined in (22), (23) and (21), respectively.

Therefore, to further simplify the objective function (24a),

$$\begin{aligned}
&\log(1+\gamma_k^B) = \max_{\omega_{B_k}\geq 0,\beta_k} \log(\omega_{B_k}) - \omega_{B_k} e_k + 1 \\
&= \max_{\omega_{B_k}\geq 0,\beta_k} \log(\omega_{B_k}) - \omega_{B_k}\big((1-\beta_k^*\mathbf{h}_k^H\mathbf{f}_k)(1-\beta_k^*\mathbf{h}_k^H\mathbf{f}_k)^H + |\beta_k|^2(\sum\nolimits_{j\neq k}^K |\mathbf{h}_k^H\mathbf{f}_j|^2 + \sigma_v^2\|\mathbf{A}\mathbf{E}_{\imath(k)}\mathbf{h}_{r,k}\|_2^2 + \sigma_{B,k}^2)\big) + 1 \\
&= \max_{\omega_{B_k}\geq 0,\beta_k} \underbrace{\log(\omega_{B_k}) - \omega_{B_k} + 2\omega_{B_k}\mathrm{Re}\{\beta_k^*\mathbf{h}_k^H\mathbf{f}_k\} - \omega_{B_k}|\beta_k|^2\sum\nolimits_{j=1}^K |\mathbf{h}_k^H\mathbf{f}_j|^2 - \omega_{B_k}|\beta_k|^2\sigma_v^2\|\mathbf{A}\mathbf{E}_{\imath(k)}\mathbf{h}_{r,k}\|_2^2 - \omega_{B_k}|\beta_k|^2\sigma_{B,k}^2 + 1}_{f_{B_k}}, \quad (22)
\end{aligned}$$

$$f_{E1_{k,l}} = \min_{\omega_{E_{k,l}}>0} \underbrace{\omega_{E_{k,l}}\big(1 + (\sum\nolimits_{j=1}^K |\mathbf{g}_l^H\mathbf{f}_j|^2 + \sigma_v^2\|\mathbf{A}\mathbf{E}_{\imath(l)}\mathbf{g}_{r,l}\|_2^2)\sigma_{E,l}^{-2}\big) - \log(\omega_{E_{k,l}}) - 1}_{\hat{f}_{E1_{k,l}}}. \quad (23)$$

we introduce slack variables $\mathbf{t} = [t_1, \ldots, t_K]^T$ and $\mathcal{C}^{K\times L} \ni \bar{\mathbf{T}} = [\bar{t}_{1,l}, \ldots, \bar{t}_{1,L}; \bar{t}_{2,l}, \ldots, \bar{t}_{2,L}; \bar{t}_{K,l}, \ldots, \bar{t}_{K,L}]$ to rewrite the problem (P1) as follows

$$(\mathrm{P2}): \max_{\substack{\{\mathbf{f}_k\},\boldsymbol{\alpha},\boldsymbol{\varsigma},\boldsymbol{\phi}_R,\boldsymbol{\phi}_T,\\ \boldsymbol{\omega}_B,\boldsymbol{\beta},\boldsymbol{\Omega}_E,\mathbf{t},\bar{\mathbf{T}}}} \sum\nolimits_{k=1}^K \{f_{B_k} - t_k\} \quad (25a)$$

$$\text{s.t.}(14b)-(14g),$$

$$\omega_{E_{k,l}}\big(\sum\nolimits_{j=1}^K |\mathbf{g}_l^H\mathbf{f}_j|^2 + \sigma_v^2\|\mathbf{A}\mathbf{E}_{\imath(l)}\mathbf{g}_{r,l}\|_2^2\big)\sigma_{E,l}^{-2} + \bar{\omega}_{E_{k,l}} - \log(1+\bar{t}_{k,l}\sigma_{E,l}^{-2}) \leq t_k,\ \forall k,\ \forall l, \quad (25b)$$

$$\bar{t}_{k,l} \leq \sum\nolimits_{j\neq k}^K |\mathbf{g}_l^H\mathbf{f}_j|^2 + \sigma_v^2\|\mathbf{A}\mathbf{E}_{\imath(l)}\mathbf{g}_{r,l}\|_2^2,\ \forall k,\ \forall l, \quad (25c)$$

where $\bar{\omega}_{E_{k,l}} \triangleq \omega_{E_{k,l}} - \log(\omega_{E_{k,l}}) - 1$.

To efficiently solve (P2), we adopt block coordinate ascent (BCA) method to alternatively update different blocks of variables, as will be elaborated in the sequel.

B. Optimizing The Auxiliary Variables $\{\beta_k\}$, $\{\omega_{B_k}\}$, $\{\omega_{E_{k,l}}\}$

i) *Updating* $\{\beta_k\}$: With other variables being fixed, the MSE function (20) is convex with respect to β_k. By checking the first-order optimality condition of β_k in (20), we can obtain the analytical solution of β_k as

$$\beta_k = \big(\sum\nolimits_{j=1}^K |\mathbf{h}_k^H\mathbf{f}_j|^2 + \sigma_v^2\|\mathbf{A}\mathbf{E}_{\imath(k)}\mathbf{h}_{r,k}\|_2^2 + \sigma_{B,k}^2\big)^{-1}\mathbf{h}_k^H\mathbf{f}_k. \quad (26)$$

ii) *Updating* $\{\omega_{E_{k,l}}\}$ *and* $\{\omega_{B_k}\}$: According to *Fact-1* of Lemma 1, with other variables being fixed, the analytical solutions of $\{\omega_{E_{k,l}}\}$ and $\{\omega_{B_k}\}$ can be respectively given as

$$\omega_{E_{k,l}} = \big(1 + (\sum\nolimits_{j=1}^K |\mathbf{g}_l^H\mathbf{f}_j|^2 + \sigma_v^2\|\mathbf{A}\mathbf{E}_{\imath(l)}\mathbf{g}_{r,l}\|_2^2)\sigma_{E,l}^{-2}\big)^{-1}, \quad (27)$$

$$\omega_{B_k} = \big(|1-\beta_k^*\mathbf{h}_k^H\mathbf{f}_k|^2 + |\beta_k|^2(\sum\nolimits_{j\neq k}^K |\mathbf{h}_k^H\mathbf{f}_j|^2 + \sigma_v^2\|\mathbf{A}\mathbf{E}_{\imath(k)}\mathbf{h}_{r,k}\|_2^2 + \sigma_{B,k}^2)\big)^{-1}. \quad (28)$$

C. Updating the AP's Beamformer $\{\mathbf{f}_k\}$

In this subsection, we present the method to update the beamformers $\{\mathbf{f}_k\}$ and the slack variables $\mathbf{t}$ and $\bar{\mathbf{T}}$. With other variables being fixed, the problem (P2) is reduced to solving the following problem

$$(\mathrm{P3}): \min_{\{\mathbf{f}_k\},\mathbf{t},\bar{\mathbf{T}}} \sum\nolimits_{k=1}^K (\mathbf{f}_k^H\bar{\mathbf{Q}}\mathbf{f}_k - 2\mathrm{Re}\{\bar{\mathbf{q}}_k^H\mathbf{f}_k\} + t_k) \quad (29a)$$

$$\text{s.t.}\sum\nolimits_{k=1}^K \|\mathbf{f}_k\|_2^2 \leq P_{AP}, \quad (29b)$$

$$\sum\nolimits_{k=1}^K \|\mathbf{A}\mathbf{G}\mathbf{f}_k\|_2^2 + \sigma_v^2\|\mathbf{A}\|_F^2 \leq P_r, \quad (29c)$$

$$\alpha_m\sum\nolimits_{k=1}^K |\bar{\mathbf{g}}_m^T\mathbf{f}_k|^2 + \alpha_m\sigma_v^2 \leq P_m, \forall m, \quad (29d)$$

$$\sum\nolimits_{j=1}^K \mathbf{f}_j^H\hat{\mathbf{Q}}_{k,l}\mathbf{f}_j + c_{1_{k,l}} - \log(1+\bar{t}_{k,l}\sigma_{E_{k,l}}^{-2}) \leq t_k,\ \forall k,\ \forall l, \quad (29e)$$

$$\bar{t}_{k,l} \leq \sum\nolimits_{j\neq k}^K \mathbf{f}_j^H\mathbf{g}_l\mathbf{g}_l^H\mathbf{f}_j + c_{2_{k,l}},\ \forall k,\ \forall l, \quad (29f)$$

where the newly introduced parameters in the above are defined as

$$\begin{aligned}
&\bar{\mathbf{Q}} \triangleq (\sum\nolimits_{k=1}^K \omega_{B_k}|\beta_k|^2\mathbf{h}_k\mathbf{h}_k^H),\ \hat{\mathbf{Q}}_{k,l} \triangleq (\omega_{E_{k,l}}\mathbf{g}_l\mathbf{g}_l^H\sigma_{E_{k,l}}^{-2}),\\
&c_{1_{k,l}} \triangleq \omega_{E_{k,l}}\sigma_v^2\|\mathbf{A}\mathbf{E}_{\imath(l)}\mathbf{g}_{r,l}\|_2^2\sigma_{E_{k,l}}^{-2} + \bar{\omega}_{E_{k,l}},\\
&c_{2_{k,l}} \triangleq \sigma_v^2\|\mathbf{A}\mathbf{E}_{\imath(l)}\mathbf{g}_{r,l}\|_2^2,\ \bar{\mathbf{q}}_k \triangleq \omega_{B_k}\beta_k\mathbf{h}_k.
\end{aligned} \quad (30)$$

The problem (P3) is still difficult to solve due to the non-convex constraint (29f). Inspired by the MM framework [42], we convexify the constraint (29f) via linearization as follows

$$\begin{aligned}
\mathbf{f}_j^H\mathbf{g}_l\mathbf{g}_l^H\mathbf{f}_j &\geq 2\mathrm{Re}\{\hat{\mathbf{f}}_j^H\mathbf{g}_l\mathbf{g}_l^H(\mathbf{f}_j - \hat{\mathbf{f}}_j)\} + \hat{\mathbf{f}}_j^H\mathbf{g}_l\mathbf{g}_l^H\hat{\mathbf{f}}_j\\
&= 2\mathrm{Re}\{\tilde{\mathbf{q}}_{j,l}\mathbf{f}_j\} - (\hat{\mathbf{f}}_j^H\mathbf{g}_l\mathbf{g}_l^H\hat{\mathbf{f}}_j)^*,
\end{aligned} \quad (31)$$

where $\tilde{\mathbf{q}}_{j,l} = \hat{\mathbf{f}}_j^H\mathbf{g}_l\mathbf{g}_l^H$ and $\{\hat{\mathbf{f}}_k\}$ are feasible solutions obtained in the last iteration. Therefore, we turn to replace the constraint (29f) by (31), the problem (P3) is rewritten as

$$(\mathrm{P4}): \min_{\{\mathbf{f}_k\},\mathbf{t},\bar{\mathbf{T}}} \sum\nolimits_{k=1}^K (\mathbf{f}_k^H\bar{\mathbf{Q}}\mathbf{f}_k - 2\mathrm{Re}\{\bar{\mathbf{q}}_k^H\mathbf{f}_k\} + t_k) \quad (32a)$$

$$\text{s.t.}(29b)-(29e),$$

$$\bar{t}_{k,l} \leq \sum\nolimits_{j\neq k}^K 2\mathrm{Re}\{\tilde{\mathbf{q}}_{j,l}\mathbf{f}_j\} + \bar{c}_{2_{k,l}},\ \forall k,\ \forall l, \quad (32b)$$

where $\bar{c}_{2_{k,l}} = c_{2_{k,l}} - \sum_{j\neq k}^K (\hat{\mathbf{f}}_j^H\mathbf{g}_l\mathbf{g}_l^H\hat{\mathbf{f}}_j)^*$. The problem (P4) is a second order cone program (SOCP) and can be efficiently solved via standard numerical solver, such as CVX [43].

D. Optimizing The Power Amplifier Coefficients

Next, we discuss the update of the power-splitting factors $\boldsymbol{\alpha}$. For simplicity, we first introduce the new definitions $\xi_{k,j} \triangleq \mathbf{f}_j^H\mathbf{h}_{d,k}$, $\boldsymbol{\tau}_{k,j} \triangleq \mathrm{Diag}(\mathbf{h}_{r,k}^*)\boldsymbol{\Phi}_{\imath(k)}\mathbf{E}_{\imath(k)}\mathbf{G}\mathbf{f}_j$, $\mathbf{k}_k \triangleq \mathbf{E}_{\imath(k)}\mathbf{h}_{r,k}$ and $\tilde{\boldsymbol{\tau}}_k \triangleq \mathrm{Diag}(\mathbf{k}_k^*)\boldsymbol{\Phi}_{\imath(k)}\mathbf{G}\mathbf{f}_k$. We rewrite the function f_{B_k} as follows

$$\begin{aligned}
&-\sum\nolimits_{k=1}^K f_{B_k}\\
&= \sqrt{\boldsymbol{\alpha}}^H\sum\nolimits_{k=1}^K \omega_{B_K}|\beta_k|^2\big(\sum\nolimits_{j=1}^K \boldsymbol{\tau}_{k,j}\boldsymbol{\tau}_{k,j}^H + \sigma_v^2\mathrm{Diag}(|\mathbf{k}_k|^2)\big)\sqrt{\boldsymbol{\alpha}}
\end{aligned}$$

$$+2\mathrm{Re}\{(\sum_{k=1}^{K}\omega_{B_k}(|\beta_k|^2(\sum_{j=1}^{K}\boldsymbol{\tau}_{k,j}\xi_{k,j})-\beta_k^*\tilde{\boldsymbol{\tau}}_k))^H\sqrt{\boldsymbol{\alpha}}\}+c_3$$
$$\triangleq \sqrt{\boldsymbol{\alpha}}^H\mathbf{Z}\sqrt{\boldsymbol{\alpha}}+2\mathrm{Re}\{\mathbf{z}^H\sqrt{\boldsymbol{\alpha}}\}+c_3. \quad (33)$$

where $\sqrt{\cdot}$, $|\cdot|$, and $(\cdot)^2$ are all element-wise operations, $\mathbf{Z}$ and $\mathbf{z}$ can be determined accordingly and c_3 is a constant irrelevant of $\boldsymbol{\alpha}$. Similarly, we again introduce $\eta_{l,j}\triangleq\mathbf{f}_j^H\mathbf{g}_{d,l}$ and $\boldsymbol{\kappa}_{l,j}\triangleq\mathrm{Diag}(\mathbf{g}_{r,l}^*)\boldsymbol{\Phi}_{i(l)}\mathbf{E}_{i(l)}\mathbf{G}\mathbf{f}_j$. The constraints (25b) and (25c) can also be rearranged into an explicit form with respect to $\boldsymbol{\alpha}$ in the following

$$\omega_{E_{k,l}}(\sum_{j=1}^{K}|\mathbf{g}_l^H\mathbf{f}_j|^2+\sigma_v^2\|\mathbf{A}\mathbf{E}_{\imath(l)}\mathbf{g}_{r,l}\|_2^2)\sigma_{E,l}^{-2}+\bar{\omega}_{E_{k,l}}$$
$$\triangleq\sqrt{\boldsymbol{\alpha}}^H\bar{\mathbf{Z}}_{k,l}\sqrt{\boldsymbol{\alpha}}+2\mathrm{Re}\{\bar{\mathbf{z}}_{k,l}^H\sqrt{\boldsymbol{\alpha}}\}+c_{4_{k,l}}, \quad (34)$$
$$\sum_{j\neq k}^{K}|\mathbf{g}_l^H\mathbf{f}_j|^2+\sigma_v^2\|\mathbf{A}\mathbf{E}_{\imath(l)}\mathbf{g}_{r,l}\|_2^2$$
$$\triangleq\sqrt{\boldsymbol{\alpha}}^H\tilde{\mathbf{Z}}_{k,l}\sqrt{\boldsymbol{\alpha}}+2\mathrm{Re}\{\tilde{\mathbf{z}}_{k,l}^H\sqrt{\boldsymbol{\alpha}}\}+c_{5_{k,l}}, \quad (35)$$

with the parameters in (34) and (35) defined as follows

$$c_{4_{k,l}}\triangleq\omega_{E_{k,l}}(\sum_{j=1}^{K}|\eta_{l,j}|^2)\sigma_{E,l}^{-2}+\bar{\omega}_{E_{k,l}},\ c_{5_{k,l}}\triangleq\sum_{j\neq k}^{K}|\eta_{l,j}|^2,$$
$$\bar{\mathbf{Z}}_{k,l}\triangleq\omega_{E_{k,l}}(\sum_{j=1}^{K}\boldsymbol{\kappa}_{l,j}\boldsymbol{\kappa}_{l,j}^H+\sigma_v^2\mathrm{Diag}(|\mathbf{E}_{\imath(l)}\mathbf{g}_{r,l}|^2))\sigma_{E,l}^{-2},$$
$$\bar{\mathbf{z}}_{k,l}\triangleq\omega_{E_{k,l}}(\sum_{j=1}^{K}\boldsymbol{\kappa}_{l,j}\eta_{l,j})\sigma_{E,l}^{-2},\ \tilde{\mathbf{z}}_{k,l}\triangleq\sum_{j\neq k}^{K}\boldsymbol{\kappa}_{l,j}\eta_{l,j},$$
$$\tilde{\mathbf{Z}}_{k,l}\triangleq(\sum_{j\neq k}^{K}\boldsymbol{\kappa}_{l,j}\boldsymbol{\kappa}_{l,j}^H)+\sigma_v^2\mathrm{Diag}(|\mathbf{E}_{\imath(l)}\mathbf{g}_{r,l}|^2). \quad (36)$$

Based on the above equivalent transformation, the amplifying coefficient $\boldsymbol{\alpha}$ should be updated via solving the following problem

$$(\mathrm{P5}):\min_{\boldsymbol{\alpha},\mathbf{t},\bar{\mathbf{T}}}\ \sqrt{\boldsymbol{\alpha}}^H\mathbf{Z}\sqrt{\boldsymbol{\alpha}}+2\mathrm{Re}\{\mathbf{z}^H\sqrt{\boldsymbol{\alpha}}\}+z+\sum_{k=1}^{K}t_k \quad (37a)$$
$$\text{s.t. }\sqrt{\boldsymbol{\alpha}}^H(\sum_{k=1}^{K}\mathrm{Diag}(|\mathbf{G}\mathbf{f}_k|^2)+\sigma_v^2\mathbf{I})\sqrt{\boldsymbol{\alpha}}\leq P_r, \quad (37b)$$
$$\alpha_m(\sum_{k=1}^{K}|\bar{\mathbf{g}}_m^T\mathbf{f}_k|^2+\sigma_v^2)\leq P_m,\forall m, \quad (37c)$$
$$\sqrt{\boldsymbol{\alpha}}^H\bar{\mathbf{Z}}_{k,l}\sqrt{\boldsymbol{\alpha}}+2\mathrm{Re}\{\bar{\mathbf{z}}_{k,l}^H\sqrt{\boldsymbol{\alpha}}\}+c_{4_{k,l}}$$
$$-\log(1+\bar{t}_{k,l}\sigma_{E,l}^{-2})\leq t_k,\ \forall k,\ \forall l, \quad (37d)$$
$$\bar{t}_{k,l}\leq\sqrt{\boldsymbol{\alpha}}^H\tilde{\mathbf{Z}}_{k,l}\sqrt{\boldsymbol{\alpha}}+2\mathrm{Re}\{\tilde{\mathbf{z}}_{k,l}^H\sqrt{\boldsymbol{\alpha}}\}+c_{5_{k,l}},\ \forall k,\ \forall l, \quad (37e)$$
$$\boldsymbol{\alpha}\geq\mathbf{0}. \quad (37f)$$

The problem (P5) is non-convex due to the constraint (37e). Noticing that the right hand side of (37e) is convex in $\sqrt{\boldsymbol{\alpha}}$, we convexify the constraint (37e) through linearization and turn the problem (P5) to convex as follows

$$(\mathrm{P6}):\min_{\boldsymbol{\alpha},\mathbf{t},\bar{\mathbf{T}}}\ \sqrt{\boldsymbol{\alpha}}^H\mathbf{Z}\sqrt{\boldsymbol{\alpha}}+2\mathrm{Re}\{\mathbf{z}^H\sqrt{\boldsymbol{\alpha}}\}+z+\sum_{k=1}^{K}t_k \quad (38a)$$
$$\text{s.t.}(37\text{b}),(37\text{c}),(37\text{d}),(37\text{f}),$$
$$\bar{t}_{k,l}\leq 2\mathrm{Re}\{(\sqrt{\hat{\boldsymbol{\alpha}}}^H\tilde{\mathbf{Z}}_{k,l}+\tilde{\mathbf{z}}_{k,l}^H)\sqrt{\boldsymbol{\alpha}}\}+\bar{c}_{5_{k,l}},\ \forall k,\ \forall l, \quad (38b)$$

where $\bar{c}_{5_{k,l}}\triangleq c_{5_{k,l}}-(\sqrt{\boldsymbol{\alpha}}^H\tilde{\mathbf{Z}}_{k,l}\sqrt{\boldsymbol{\alpha}})^*$ and $\hat{\boldsymbol{\alpha}}$ is obtained from the last iteration. Besides, it is obvious that the problem (P6) is an SOCP and can be solved by CVX.

E. Optimizing The Power Splitting Coefficients $\boldsymbol{\varsigma}$

In this subsection, we investigate the update of power splitting coefficients $\boldsymbol{\varsigma}$ when other variables are given. Firstly, the function f_{B_k}, which is defined in (22), is rewritten as

$$-\sum_{k=1}^{K}f_{B_k}=\sum_{\imath\in\{R,T\}}(\mathbf{e}_\imath^H\mathbf{S}_\imath\mathbf{e}_\imath+2\mathrm{Re}\{\mathbf{s}_\imath^H\mathbf{e}_\imath\})+c_6, \quad (39)$$

where c_6 is a constant and the above newly introduced coefficients are defined as

$$\mathbf{e}_{\imath(k\text{ or }l)}\triangleq\begin{cases}\boldsymbol{\varsigma} & \text{if } k\in\mathcal{K}_R \text{ or } l\in\mathcal{L}_R\\ \sqrt{1-\boldsymbol{\varsigma}^2} & \text{if } k\in\mathcal{K}_T \text{ or } l\in\mathcal{L}_T\end{cases},$$
$$\boldsymbol{\chi}_{k,j}\triangleq\mathrm{Diag}(\mathbf{h}_{r,k}^*)\boldsymbol{\Phi}_{\imath(k)}\mathbf{A}\mathbf{G}\mathbf{f}_j,$$
$$\mathbf{Q}_\imath\triangleq\sum_{k\in\mathcal{K}_\imath}\omega_{B_k}|\beta_k|^2(\sum_{j=1}^{K}\boldsymbol{\chi}_{k,j}\boldsymbol{\chi}_{k,j}^H),\ \imath\in\{R,T\},$$
$$\mathbf{q}_\imath\triangleq\sum_{k\in\mathcal{K}_\imath}\omega_{B_k}|\beta_k|^2(\sum_{j=1}^{K}\xi_{k,j}\boldsymbol{\chi}_{k,j}),\ \imath\in\{R,T\},$$
$$\mathbf{d}_\imath\triangleq\sum_{k\in\mathcal{K}_\imath}\omega_{B_k}\beta_k^*\mathrm{Diag}(\mathbf{h}_{r,k}^*)\boldsymbol{\Phi}_{\imath(k)}\mathbf{A}\mathbf{G}\mathbf{f}_k,\ \imath\in\{R,T\},$$
$$\mathbf{D}_\imath\triangleq\sum_{k\in\mathcal{K}_\imath}\omega_{B_k}|\beta_k|^2\sigma_v^2\mathrm{Diag}(|\mathbf{A}\mathbf{h}_{r,k}|^2),\ \imath\in\{R,T\},$$
$$\mathbf{S}_\imath\triangleq\mathbf{Q}_\imath+\mathbf{D}_\imath,\ \mathbf{s}_\imath\triangleq\mathbf{q}_\imath-\mathbf{d}_\imath,\ \imath\in\{R,T\}. \quad (40)$$

Similarly, by denoting $\boldsymbol{\nu}_{l,j}\triangleq\mathrm{Diag}(\mathbf{g}_{r,l}^*)\boldsymbol{\Phi}_{\imath(l)}\mathbf{A}\mathbf{G}\mathbf{f}_j$, the $\boldsymbol{\varsigma}$ relevant terms in (25b) and (25c) can be rewritten as

$$\omega_{E_{k,l}}(\sum_{j=1}^{K}|\mathbf{g}_l^H\mathbf{f}_j|^2+\sigma_v^2\|\mathbf{A}\mathbf{E}_{\imath(l)}\mathbf{g}_{r,l}\|_2^2)\sigma_{E,l}^{-2}+\bar{\omega}_{E_{k,l}}$$
$$=\mathbf{e}_\imath^H\mathbf{U}_{k,l}\mathbf{e}_\imath+2\mathrm{Re}\{\mathbf{u}_{k,l}^H\mathbf{e}_\imath\}+c_{7_{k,l}},\ \imath\in\{R,T\}, \quad (41)$$
$$\sum_{j\neq k}^{K}|\mathbf{g}_l^H\mathbf{f}_j|^2+\sigma_v^2\|\mathbf{A}\mathbf{E}_{\imath(l)}\mathbf{g}_{r,l}\|_2^2$$
$$=\mathbf{e}_\imath^H\bar{\mathbf{U}}_{k,l}\mathbf{e}_\imath+2\mathrm{Re}\{\bar{\mathbf{u}}_{k,l}^H\mathbf{e}_\imath\}+c_{8_{k,l}},\ \imath\in\{R,T\}. \quad (42)$$

with the parameters in (41) and (42) being defined as follows

$$\mathbf{u}_{k,l}\triangleq\omega_{E_{k,l}}(\sum_{j=1}^{K}\eta_{l,j}\boldsymbol{\nu}_{l,j})\sigma_{E,l}^{-2}, c_{7_{k,l}}\triangleq\omega_{E_{k,l}}(\sum_{j=1}^{K}|\eta_{l,j}|^2)\sigma_{E,l}^{-2},$$
$$\mathbf{U}_{k,l}\triangleq\omega_{E_{k,l}}(\sum_{j=1}^{K}\boldsymbol{\nu}_{l,j}\boldsymbol{\nu}_{l,j}^H+\sigma_v^2\mathrm{Diag}(|\mathbf{A}\mathbf{g}_{r,l}|^2))\sigma_{E,l}^{-2},$$
$$\bar{\mathbf{U}}_{k,l}\triangleq\sum_{j\neq k}^{K}\boldsymbol{\nu}_{l,j}\boldsymbol{\nu}_{l,j}^H+\sigma_v^2\mathrm{Diag}(|\mathbf{A}\mathbf{g}_{r,l}|^2),$$
$$\bar{\mathbf{u}}_{k,l}\triangleq\sum_{j\neq k}^{K}\eta_{l,j}\boldsymbol{\nu}_{l,j},\ c_{8_{k,l}}=\sum_{j\neq k}^{K}|\eta_{l,j}|^2. \quad (43)$$

Therefore, the power splitting coefficients optimization reduces to solving the following problem

$$(\mathrm{P7}):\min_{\boldsymbol{\varsigma},\mathbf{t},\bar{\mathbf{T}}}\ \boldsymbol{\varsigma}^H\mathbf{S}_R\boldsymbol{\varsigma}+\sqrt{1-\boldsymbol{\varsigma}^2}^H\mathbf{S}_T\sqrt{1-\boldsymbol{\varsigma}^2} \quad (44a)$$
$$+2\mathrm{Re}\{\mathbf{s}_R^H\boldsymbol{\varsigma}+\mathbf{s}_T^H\sqrt{1-\boldsymbol{\varsigma}^2}\}+\sum_{k=1}^{K}t_k+c_6$$
$$\text{s.t.}\boldsymbol{\varsigma}^H\mathbf{U}_{k,l}\boldsymbol{\varsigma}+2\mathrm{Re}\{\mathbf{u}_{k,l}^H\boldsymbol{\varsigma}\}+c_{7_{k,l}}$$
$$-\log(1+\bar{t}_{k,l}\sigma_{E,l}^{-2})\leq t_k,\ \forall k,\ \forall l\in\mathcal{L}_R, \quad (44b)$$
$$\sqrt{1-\boldsymbol{\varsigma}^2}^H\mathbf{U}_{k,l}\sqrt{1-\boldsymbol{\varsigma}^2}+2\mathrm{Re}\{\mathbf{u}_{k,l}^H\sqrt{1-\boldsymbol{\varsigma}^2}\}$$
$$+c_{7_{k,l}}-\log(1+\bar{t}_{k,l}\sigma_{E,l}^{-2})\leq t_k,\ \forall k,\ \forall l\in\mathcal{L}_T, \quad (44c)$$
$$\bar{t}_{k,l}\leq\boldsymbol{\varsigma}^H\bar{\mathbf{U}}_{k,l}\boldsymbol{\varsigma}+2\mathrm{Re}\{\bar{\mathbf{u}}_{k,l}^H\boldsymbol{\varsigma}\}+c_{8_{k,l}},\ \forall k,\ \forall l\in\mathcal{L}_R, \quad (44d)$$
$$\bar{t}_{k,l}\leq\sqrt{1-\boldsymbol{\varsigma}^2}^H\bar{\mathbf{U}}_{k,l}\sqrt{1-\boldsymbol{\varsigma}^2}$$
$$+2\mathrm{Re}\{\bar{\mathbf{u}}_{k,l}^H\sqrt{1-\boldsymbol{\varsigma}^2}\}+c_{8_{k,l}},\ \forall k,\ \forall l\in\mathcal{L}_T, \quad (44e)$$
$$0\leq\varsigma_m\leq 1,\ \forall m. \quad (44f)$$

Obviously, the non-convex term $\sqrt{1-\boldsymbol{\varsigma}^2}$ in (44a), (44c) and (44e), makes the problem (P7) intractable. In the following,

This article has been accepted for publication in IEEE Transactions on Communications. This is the author's version which has not been fully edited and content may change prior to final publication. Citation information: DOI 10.1109/TCOMM.2023.3250454

we adopt the MM methodology to resolve this difficulty.

Firstly, for any positive semidefinite matrix $\mathbf{E}$, we have the following inequality

$$\begin{aligned}&\mathbf{e}_T^H\mathbf{E}\mathbf{e}_T \quad (45)\\&=(\mathbf{e}_T-\mathbf{e}_{T,0})^H\mathbf{E}(\mathbf{e}_T-\mathbf{e}_{T,0})+2\mathrm{Re}\{\mathbf{e}_{T,0}^H\mathbf{E}(\mathbf{e}_T-\mathbf{e}_{T,0})\}+\mathbf{e}_{T,0}^H\mathbf{E}\mathbf{e}_{T,0}\\&\le\lambda_{max}(\mathbf{E})\|\mathbf{e}_T-\mathbf{e}_{T,0}\|_2^2+2\mathrm{Re}\{\mathbf{e}_{T,0}^H\mathbf{E}(\mathbf{e}_T-\mathbf{e}_{T,0})\}+\mathbf{e}_{T,0}^H\mathbf{E}\mathbf{e}_{T,0}\\&=\lambda_{max}(\mathbf{E})\|\mathbf{e}_T\|_2^2+2\mathrm{Re}\{(\mathbf{E}\mathbf{e}_{T,0}-\lambda_{max}(\mathbf{E})\mathbf{e}_{T,0})^H\mathbf{e}_T\}+c_9,\end{aligned}$$

with $\lambda_{max}(\mathbf{E})$ being the maximal eigenvalue of $\mathbf{E}$, c_9 is a constant, $\mathbf{e}_0 \triangleq \sqrt{1-\boldsymbol{\varsigma}_0^2}$ and ς_0 is the latest value of ς. Therefore, following the arguments presented in (45), we can construct tight upper-bounds for (44a) and (44c), as will be clarified in the following. Specifically, the term $\sqrt{1-\boldsymbol{\varsigma}^2}$ in (44a) can be upper-bounded as follows

$$\begin{aligned}&\mathbf{e}_R^H\mathbf{S}_R\mathbf{e}_R+\mathbf{e}_T^H\mathbf{S}_T\mathbf{e}_T+2\mathrm{Re}\{\mathbf{s}_R^H\mathbf{e}_R+\mathbf{s}_T^H\mathbf{e}_T\}+c_6 \quad (46)\\&\le\mathbf{e}_R^H\mathbf{S}_R\mathbf{e}_R+\lambda_T\|\mathbf{e}_T\|_2^2+2\mathrm{Re}\{\mathbf{s}_R^H\mathbf{e}_R\}+2\mathrm{Re}\{\bar{\mathbf{s}}_T^H\mathbf{e}_T\}+\bar{c}_6\\&=\mathbf{e}_R^H\mathbf{S}_R\mathbf{e}_R+2\mathrm{Re}\{\mathbf{s}_R^H\mathbf{e}_R\}+\sum_{m=1}^M\big(\lambda_T(1-\varsigma_m^2)+2\mathrm{Re}\{\bar{s}_{T,m}^*\sqrt{1-\varsigma_m^2}\}\big)+\bar{c}_6,\end{aligned}$$

and the $\sqrt{1-\boldsymbol{\varsigma}^2}$ term in (44c) can be upper-bounded by

$$\begin{aligned}&\mathbf{e}_T^H\mathbf{U}_{k,l}\mathbf{e}_T+2\mathrm{Re}\{\mathbf{u}_{k,l}^H\mathbf{e}_T\}+c_{7_{k,l}}\\&\le\lambda_{\mathbf{U}_{k,l}}\|\mathbf{e}_T\|_2^2+2\mathrm{Re}\{\tilde{\mathbf{u}}_{k,l}^H\mathbf{e}_T\}+\bar{c}_{7_{k,l}} \quad (47)\\&=\sum_{m=1}^M\big(\lambda_{\mathbf{U}_{k,l}}(1-\varsigma_m^2)+2\mathrm{Re}\{\tilde{u}_{k,l,m}^*\sqrt{1-\varsigma_m^2}\}\big)+\bar{c}_{7_{k,l}},\end{aligned}$$

where $\bar{c}_6$ and $\bar{c}_{7_{k,l}}$ are constant terms and the above newly introduced coefficients are defined as

$$\begin{aligned}&\lambda_T\triangleq\lambda_{max}(\mathbf{S}_T),\ \bar{\mathbf{s}}_T\triangleq\mathbf{S}_T\mathbf{e}_{T,0}-\lambda_T\mathbf{e}_{T,0}+\mathbf{s}_T, \quad (48)\\&\lambda_{\mathbf{U}_l}\triangleq\lambda_{max}(\mathbf{U}_l),\ \tilde{\mathbf{u}}_l\triangleq\mathbf{U}_l\mathbf{e}_{T,0}-\lambda_{\mathbf{U}_l}\mathbf{e}_{T,0}+\mathbf{u}_l,\ \forall l\in\mathcal{L}_T.\end{aligned}$$

Note that there still exist non-convex terms $-\lambda\varsigma_m^2$, $2\mathrm{Re}\{\bar{s}_{T,m}^*\sqrt{1-\varsigma_m^2}\}$ and $2\mathrm{Re}\{\tilde{u}_{k,l,m}^*\sqrt{1-\varsigma_m^2}\}$ in (46) and (47). To obtain convex surrogates, we further convexify these non-convex terms. Specifically, the concave terms $-\lambda\varsigma_m^2$ can be convexified by linearization as follows

$$-\lambda\varsigma_m^2\le-\lambda[\varsigma_{m,0}^2+2\varsigma_{m,0}(\varsigma_m-\varsigma_{m,0})]. \quad (49)$$

To convexify the term $2\mathrm{Re}\{\bar{s}_{T,m}^*\sqrt{1-\varsigma_m^2}\}$, two possible cases should be considered, depending on the sign of $\mathrm{Re}\{\bar{s}_{T,m}^*\}$.

case-1: $\mathrm{Re}\{\bar{s}_{T,m}^*\}\le 0$. The term $2\mathrm{Re}\{\bar{s}_{T,m}^*\sqrt{1-\varsigma_m^2}\}$ is indeed convex and therefore no operation is needed.

case-2: $\mathrm{Re}\{\bar{s}_{T,m}^*\}>0$. $2\mathrm{Re}\{\bar{s}_{T,m}^*\sqrt{1-\varsigma_m^2}\}$ is concave. Therefore, we construct an upper-bound of $2\mathrm{Re}\{\bar{s}_{T,m}^*\sqrt{1-\varsigma_m^2}\}$ at the point of $\varsigma_{m,0}$, which is given as

$$\begin{aligned}&\sqrt{1-\varsigma_m^2}\le\sqrt{1-\varsigma_{m,0}^2}-\varsigma_{m,0}\sqrt{1-\varsigma_{m,0}^2}^{-1}(\varsigma_m-\varsigma_{m,0})\\&=-(\varsigma_{m,0}\sqrt{1-\varsigma_{m,0}^2}^{-1})\varsigma_m+\sqrt{1-\varsigma_{m,0}^2}+\varsigma_{m,0}^2\sqrt{1-\varsigma_{m,0}^2}^{-1}. \quad (50)\end{aligned}$$

The terms $2\mathrm{Re}\{\tilde{u}_{k,l,m}^*\sqrt{1-\varsigma_m^2}\}$ present in (47) can be similarly convexified following the same arguments as above. By applying (49) to $-\lambda\varsigma_m^2$ and possibly invoking the convexification procedure in (50), we can obtain convex tight upper-bounds of (46) and (47) as shown in (51) and (52), respectively, in the following

$$\begin{aligned}&\mathbf{e}_R^H\mathbf{S}_R\mathbf{e}_R+\mathbf{e}_T^H\mathbf{S}_T\mathbf{e}_R+2\mathrm{Re}\{\mathbf{s}_R^H\mathbf{e}_R+\mathbf{s}_T^H\mathbf{e}_T\}+c_6 \quad (51)\\&\le\mathbf{e}_R^H\mathbf{S}_R\mathbf{e}_R+2\mathrm{Re}\{\mathbf{s}_R^H\mathbf{e}_R\}+\sum_{m=1}^M\big(b_m\varsigma_m-c_m\sqrt{1-\varsigma_m^2}\big)+\tilde{c}_6,\end{aligned}$$

$$\begin{aligned}&\mathbf{e}_T^H\mathbf{U}_{k,l}\mathbf{e}_T+2\mathrm{Re}\{\mathbf{u}_{k,l}^H\mathbf{e}_T\}+c_{7_{k,l}} \quad (52)\\&\le\sum_{m=1}^M\big(\tilde{b}_{k,l,m}\varsigma_m-\tilde{c}_{k,l,m}\sqrt{1-\varsigma_m^2}\big)+\tilde{c}_{7_{k,l}},\end{aligned}$$

with $\tilde{c}_6$ and $\tilde{c}_{7_{k,l}}$ being constants. According to the above derivations, it can be readily seen the introduced coefficients $\{b_m\}$ and $\{\tilde{b}_{k,l,m}\}$ are positive, and $\{c_m\}$ and $\{\tilde{c}_{k,l,m}\}$ are nonnegative.

After convexifying (44a) and (44c), we proceed to deal with non-convex constraint (44d). To this end, still following the MM method, we first linearize the quadratic term to obtain a tight lower bound as follows

$$\begin{aligned}&\mathbf{e}_R^H\bar{\mathbf{U}}_{k,l}\mathbf{e}_R+2\mathrm{Re}\{\bar{\mathbf{u}}_{k,l}^H\mathbf{e}_R\}+c_{8_{k,l}} \quad (53)\\&\ge\mathbf{e}_{R,0}^H\bar{\mathbf{U}}_{k,l}\mathbf{e}_{R,0}+2\mathrm{Re}\{\mathbf{e}_{R,0}\bar{\mathbf{U}}_{k,l}(\mathbf{e}_R-\mathbf{e}_{R,0})\}+2\mathrm{Re}\{\bar{\mathbf{u}}_{k,l}^H\mathbf{e}_R\}+c_{8_{k,l}}\\&=2\mathrm{Re}\{(\mathbf{e}_{R,0}^H\bar{\mathbf{U}}_{k,l}+\bar{\mathbf{u}}_{k,l}^H)\mathbf{e}_R\}+\bar{c}_{8_{k,l}},\end{aligned}$$

where $\mathbf{e}_{R,0}$ is the value obtained in the last iteration and $\bar{c}_{8_{k,l}}\triangleq-(\mathbf{e}_{R,0}^H\bar{\mathbf{U}}_{k,l}\mathbf{e}_{R,0})^*+c_{8_{k,l}}$.

To make (P7) tractable, we still need to convexify the constraint (44e). Towards this end, we rewrite by expanding vectors into entries as follows

$$\begin{aligned}&\sqrt{1-\boldsymbol{\varsigma}^2}^H\bar{\mathbf{U}}_{k,l}\sqrt{1-\boldsymbol{\varsigma}^2}+2\mathrm{Re}\{\bar{\mathbf{u}}_{k,l}^H\sqrt{1-\boldsymbol{\varsigma}^2}\}=\sum_{m=1}^M\bar{\mathrm{U}}_{k,l,m,m}(1-\varsigma_m^2)\\&+\sum_{m\neq n}\bar{\mathrm{U}}_{k,l,m,n}\sqrt{1-\varsigma_m^2}\sqrt{1-\varsigma_n^2}+\sum_{m=1}^M2\mathrm{Re}\{\bar{\mathrm{u}}_{k,l,m}^*\sqrt{1-\varsigma_m^2}\}. \quad (54)\end{aligned}$$

In the following, to obtain convex surrogate of (54) (i.e., (44e)), we investigate the convexifications of the terms $\bar{\mathrm{U}}_{k,l,m,n}\sqrt{1-\varsigma_m^2}\sqrt{1-\varsigma_n^2}$, $\bar{\mathrm{U}}_{k,l,m,m}(1-\varsigma_m^2)$ and $2\mathrm{Re}\{\bar{\mathrm{u}}_{k,l,m}^*\sqrt{1-\varsigma_m^2}\}$ in (54) in order.

Firstly, according to the sign of $\bar{\mathrm{U}}_{k,l,m,m}$, the convexity of $\bar{\mathrm{U}}_{k,l,m,m}(1-\varsigma_m^2)$ should be considered in two possible cases:

case-1: if $\bar{\mathrm{U}}_{k,l,m,m}\ge 0$. The term $\bar{\mathrm{U}}_{k,l,m,m}(1-\varsigma_m^2)$ is indeed concave and no operation is needed.

case-2: if $\bar{\mathrm{U}}_{k,l,m,m}<0$. The term $\bar{\mathrm{U}}_{k,l,m,m}(1-\varsigma_m^2)$ is convex. we linearize it at the point of $\varsigma_{m,0}$ to obtain a tight lower-bound given as follows

$$\begin{aligned}&-\bar{\mathrm{U}}_{k,l,m,m}\varsigma_m^2\ge-\bar{\mathrm{U}}_{k,l,m,m}[\varsigma_{m,0}^2+2\varsigma_{m,0}(\varsigma_m-\varsigma_{m,0})]\\&=-2\varsigma_{m,0}\bar{\mathrm{U}}_{k,l,m,m}\varsigma_m+\bar{\mathrm{U}}_{k,l,m,m}\varsigma_{m,0}^2. \quad (55)\end{aligned}$$

Different from the upper-bounding procedures used in (46) and (47), this time we need a tight concave lower bound of $2\mathrm{Re}\{\bar{\mathrm{u}}_{k,l,m}^*\sqrt{1-\varsigma_m^2}\}$. This can still be achieved via linearization (refer to (50)) when $\mathrm{Re}\{\bar{\mathrm{u}}_{k,l,m}^*\}<0$. Details are omitted to avoid repetition.

Finally, to tackle the cross terms $\bar{\mathrm{U}}_{k,l,m,n}\sqrt{1-\varsigma_m^2}\sqrt{1-\varsigma_n^2}$, we introduce the following results that are proved in [42].

Lemma 2. *Assume that ς_m, ς_n, $\varsigma_{m,0}$ and $\varsigma_{n,0}$ are arbitrary positive values. Then the following inequality hold*

$$\sqrt{\varsigma_m}\sqrt{\varsigma_n}\le\big(\sqrt{\varsigma_{n,0}/\varsigma_{m,0}}\varsigma_m+\sqrt{\varsigma_{m,0}/\varsigma_{n,0}}\varsigma_n\big)/2, \quad (56)$$

$$\begin{aligned}&\sqrt{\varsigma_m}\sqrt{\varsigma_n}\ge\sqrt{\varsigma_{m,0}}\sqrt{\varsigma_{n,0}}(\log\varsigma_m+\log\varsigma_n)/2\\&+\sqrt{\varsigma_{m,0}}\sqrt{\varsigma_{n,0}}\big(2-\log\varsigma_{m,0}+\log\varsigma_{n,0}\big)/2. \quad (57)\end{aligned}$$

By Lemma 2, we can construct concave lower-bound of the terms $\bar{\mathrm{U}}_{k,l,m,n}\sqrt{1-\varsigma_m^2}\sqrt{1-\varsigma_n^2}$, as specified in the following two possible cases:

case-1: if $\bar{\mathrm{U}}_{k,l,m,n}\ge 0$, by leveraging (57), we have

$$\sqrt{1-\varsigma_m^2}\sqrt{1-\varsigma_n^2}$$

$$\geq \frac{1}{2}\sqrt{1-\varsigma_{m,0}^2}\sqrt{1-\varsigma_{n,0}^2}(\log(1-\varsigma_m^2)+\log(1-\varsigma_n^2))$$
$$+\frac{1}{2}\sqrt{1-\varsigma_{m,0}^2}\sqrt{1-\varsigma_{n,0}^2}(2-\log(1-\varsigma_{m,0}^2)-\log(1-\varsigma_{n,0}^2)). \quad (58)$$

case-2: if $\bar{\mathrm{U}}_{k,l,m,n} < 0$, we can obtain

$$-\sqrt{1-\varsigma_m^2}\sqrt{1-\varsigma_n^2}$$
$$\overset{(a)}{\geq} -\frac{1}{2}\Big[\frac{\sqrt{1-\varsigma_{n,0}^2}}{\sqrt{1-\varsigma_{m,0}^2}}(1-\varsigma_m^2)+\frac{\sqrt{1-\varsigma_{m,0}^2}}{\sqrt{1-\varsigma_{n,0}^2}}(1-\varsigma_n^2)\Big]$$
$$\overset{(b)}{\geq} \Big[\frac{\sqrt{1-\varsigma_{n,0}^2}}{\sqrt{1-\varsigma_{m,0}^2}}\varsigma_{m,0}\varsigma_m+\frac{\sqrt{1-\varsigma_{m,0}^2}}{\sqrt{1-\varsigma_{n,0}^2}}\varsigma_{n,0}\varsigma_n\Big]$$
$$-\frac{1}{2}\Big[\frac{\sqrt{1-\varsigma_{n,0}^2}}{\sqrt{1-\varsigma_{m,0}^2}}(1+\varsigma_{m,0}^2)+\frac{\sqrt{1-\varsigma_{m,0}^2}}{\sqrt{1-\varsigma_{n,0}^2}}(1+\varsigma_{n,0}^2)\Big], \quad (59)$$

where (a) is due to (56) and (b) is due to linearizing the concave terms $-\varsigma^2$.

In the above, $\varsigma_{m,0}$ and $\varsigma_{n,0}$ are chosen as the values obtained in the last iteration.

By replacing the non-concave terms $\bar{\mathrm{U}}_{k,l,m,m}(1-\varsigma_m^2)$, $\bar{\mathrm{U}}_{k,l,m,n}\sqrt{1-\varsigma_m^2}\sqrt{1-\varsigma_n^2}$ and $2\mathrm{Re}\{\bar{\mathrm{u}}_{k,l,m}^*\sqrt{1-\varsigma_m^2}\}$ in (54) with their associated lower-bounds developed above, we obtain a concave surrogate of (54) as follows

$$\sqrt{1-\boldsymbol{\varsigma}^2}^H\bar{\mathbf{U}}_{k,l}\sqrt{1-\boldsymbol{\varsigma}^2}+2\mathrm{Re}\{\bar{\mathbf{u}}_{k,l}^H\sqrt{1-\boldsymbol{\varsigma}^2}\}+c_{8_{k,l}}$$
$$\geq \sum_{m=1}^{M}\big(-\bar{a}_{k,l,m}\varsigma_m^2+\bar{b}_{k,l,m}\varsigma_m+\bar{c}_{k,l,m}\sqrt{1-\varsigma_m^2}$$
$$-\bar{d}_{k,l,m}\log(1-\varsigma_m^2)\big)+\tilde{c}_{8_{k,l}}, \quad (60)$$

with $\tilde{c}_{8_{k,l}}$ being constant and the coefficients $\{\bar{a}_{k,l,m}\}$, $\{\bar{b}_{k,l,m}\}$, $\{\bar{c}_{k,l,m}\}$ and $\{\bar{d}_{k,l,m}\}$ being accordingly determined. Obviously, $\bar{a}_{k,l,m}\geq 0$, $\bar{b}_{k,l,m}>0$, $\bar{c}_{k,l,m}\geq 0$ and $\bar{d}_{k,l,m}\geq 0$, $\forall m\in\mathcal{M}$.

Following the MM transformation presented above, the update of $\boldsymbol{\varsigma}$ can be conducted via solving a convexified surrogate of the original difficult problem (P7) given as follows

$$(\mathrm{P8}): \min_{\boldsymbol{\varsigma},\mathbf{t},\bar{\mathbf{T}}} \ \boldsymbol{\varsigma}^H\mathbf{S}_R\boldsymbol{\varsigma}+2\mathrm{Re}\{\mathbf{s}_R^H\boldsymbol{\varsigma}\}$$
$$+\sum_{m=1}^{M}\big(b_m\varsigma_m-c_m\sqrt{1-\varsigma_m^2}\big)+c_6+\sum_{k=1}^{K}t_k \quad (61a)$$
$$\text{s.t. } \boldsymbol{\varsigma}^H\mathbf{U}_l\boldsymbol{\varsigma}+2\mathrm{Re}\{\mathbf{u}_l^H\boldsymbol{\varsigma}\}+c_{7_{k,l}}$$
$$-\log(1+\bar{t}_{k,l}\sigma_{E,l}^{-2})\leq t_k,\ \forall k,\ \forall l\in\mathcal{L}_R, \quad (61b)$$
$$\sum_{m=1}^{M}\big(\tilde{b}_{k,l,m}\varsigma_m-\tilde{c}_{k,l,m}\sqrt{1-\varsigma_m^2}\big)+\tilde{c}_{7_{k,l}}$$
$$-\log(1+\bar{t}_{k,l}\sigma_{E,l}^{-2})\leq t_k,\ \forall k,\ \forall l\in\mathcal{L}_T, \quad (61c)$$
$$\bar{t}_{k,l}\leq 2\mathrm{Re}\{(\boldsymbol{\varsigma}_0^H\bar{\mathrm{U}}_{k,l}+\bar{\mathbf{u}}_{k,l}^H)\boldsymbol{\varsigma}\}+\bar{c}_{8_{k,l}},\ \forall k,\ \forall l\in\mathcal{L}_R, \quad (61d)$$
$$\bar{t}_{k,l}\leq \sum_{m=1}^{M}\big(-\bar{a}_{k,l,m}\varsigma_m^2+\bar{b}_{k,l,m}\varsigma_m+\bar{c}_{k,l,m}\sqrt{1-\varsigma_m^2}$$
$$-\bar{d}_{k,l,m}\log(1-\varsigma_m^2)\big)+\tilde{c}_{8_{k,l}},\ \forall k,\ \forall l\in\mathcal{L}_T, \quad (61e)$$
$$0\leq\varsigma_m\leq 1,\ \forall m. \quad (61f)$$

The problem (P8) can be efficiently solved via CVX.

F. Optimizing The Phase Shifts

In this subsection, we investigate the optimization of the phase shifts $\boldsymbol{\phi}_R$ and $\boldsymbol{\phi}_T$. By denoting $\boldsymbol{\varpi}_{k,j} \triangleq \mathrm{Diag}(\mathbf{h}_{r,k}^*)\mathbf{E}_{\imath(k)}\mathbf{AGf}_j$, we rewrite the functions f_{B_k} in (P2) as follows

$$-\sum_{k=1}^{K}f_{B_k}=\boldsymbol{\phi}_R^H\mathbf{P}_R\boldsymbol{\phi}_R+2\mathrm{Re}\{\mathbf{p}_R^H\boldsymbol{\phi}_R\}$$
$$+\boldsymbol{\phi}_T^H\mathbf{P}_T\boldsymbol{\phi}_T+2\mathrm{Re}\{\mathbf{p}_T^H\boldsymbol{\phi}_T\}+c_9, \quad (62)$$

where c_9 is a constant and the new parameters in the above are defined as

$$\mathbf{P}_\imath \triangleq \sum_{k\in\mathcal{K}_\imath}\omega_{B_k}|\beta_k|^2\big(\sum_{j=1}^{K}\boldsymbol{\varpi}_{k,j}^*\boldsymbol{\varpi}_{k,j}^T\big),\ \imath\in\{R,T\},$$
$$\mathbf{p}_\imath \triangleq \sum_{k\in\mathcal{K}_\imath}\big(\omega_{B_k}|\beta_k|^2(\sum_{j=1}^{K}\xi_{k,j}^*\boldsymbol{\varpi}_{k,j}^*) \quad (63)$$
$$-(\omega_{B_k}\beta_k^*\mathrm{Diag}(\mathbf{h}_{r,k}^*)\mathbf{E}_{\imath(k)}\mathbf{AGf}_k)^*\big),\ \imath\in\{R,T\}.$$

Besides, the terms relevant to $\boldsymbol{\phi}_\imath$, $\imath\in\{R,T\}$, in (25b) and (25c) can be equivalently expressed as

$$\omega_{E_{k,l}}\big(\sum_{j=1}^{K}|\mathbf{g}_l^H\mathbf{f}_j|^2+\sigma_v^2\|\mathbf{AE}_{\imath(l)}\mathbf{g}_{r,l}\|_2^2\big)\sigma_{E,l}^{-2}+\bar{\omega}_{E_{k,l}}$$
$$=\boldsymbol{\phi}_{\imath(l)}^H\bar{\mathbf{P}}_{k,l}\boldsymbol{\phi}_{\imath(l)}+2\mathrm{Re}\{\bar{\mathbf{p}}_{k,l}^H\boldsymbol{\phi}_{\imath(l)}\}+c_{10_{k,l}},\ \imath\in\{R,T\}, \quad (64)$$
$$\sum_{j\neq k}^{K}|\mathbf{g}_l^H\mathbf{f}_j|^2+\sigma_v^2\|\mathbf{AE}_{\imath(l)}\mathbf{g}_{r,l}\|_2^2$$
$$=\boldsymbol{\phi}_{\imath(l)}^H\tilde{\mathbf{P}}_{k,l}\boldsymbol{\phi}_{\imath(l)}+2\mathrm{Re}\{\tilde{\mathbf{p}}_{k,l}^H\boldsymbol{\phi}_{\imath(l)}\}+c_{11_{k,l}},\ \imath\in\{R,T\}, \quad (65)$$

where the new coefficients are defined as follows

$$\bar{\mathbf{P}}_{k,l}\triangleq\sum_{j=1}^{K}\omega_{E_{k,l}}\boldsymbol{\mu}_{l,j}^*\boldsymbol{\mu}_{l,j}^T\sigma_{E,l}^{-2},\ \bar{\mathbf{p}}_{k,l}\triangleq\sum_{j=1}^{K}\omega_{E_{k,l}}\eta_{l,j}^*\boldsymbol{\mu}_{l,j}^*\sigma_{E,l}^{-2},$$
$$c_{10_{k,l}}\triangleq\omega_{E_{k,l}}\big(\sum_{j=1}^{K}|\eta_{l,j}|^2+\sigma_v^2\|\mathbf{AE}_{i(l)}\mathbf{g}_{r,l}\|_2^2\big)\sigma_{E,l}^{-2}+\bar{\omega}_{E_{k,l}},$$
$$\tilde{\mathbf{P}}_{k,l}\triangleq\sum_{j\neq k}^{K}\boldsymbol{\mu}_{l,j}^*\boldsymbol{\mu}_{l,j}^T,\ \tilde{\mathbf{p}}_{k,l}\triangleq\sum_{j\neq k}^{K}\eta_{l,j}^*\boldsymbol{\mu}_{l,j}^*,$$
$$c_{11_{k,l}}\triangleq\sum_{j\neq k}^{K}\eta_{l,j}\eta_{l,j}^*+\sigma_v^2\|\mathbf{AE}_{i(l)}\mathbf{g}_{r,l}\|_2^2. \quad (66)$$

Based on the above discussions, the update of the phase-shifts is meant to solve the following problem

$$(\mathrm{P9}): \min_{\boldsymbol{\phi}_R,\boldsymbol{\phi}_T,\mathbf{t},\bar{\mathbf{T}}} \ \boldsymbol{\phi}_R^H\mathbf{P}_R\boldsymbol{\phi}_R+2\mathrm{Re}\{\mathbf{p}_R^H\boldsymbol{\phi}_R\}$$
$$+\boldsymbol{\phi}_T^H\mathbf{P}_T\boldsymbol{\phi}_T+2\mathrm{Re}\{\mathbf{p}_T^H\boldsymbol{\phi}_T\}+\sum_{k=1}^{K}t_k+c_9 \quad (67a)$$
$$\text{s.t. } |\boldsymbol{\phi}_{\imath,m}|=1,\ \imath\in\{R,T\},\ \forall m, \quad (67b)$$
$$\boldsymbol{\phi}_{\imath(l)}^H\bar{\mathbf{P}}_{k,l}\boldsymbol{\phi}_{\imath(l)}+2\mathrm{Re}\{\bar{\mathbf{p}}_{k,l}^H\boldsymbol{\phi}_{\imath(l)}\}+c_{10_{k,l}}$$
$$-\log(1+\bar{t}_{k,l}\sigma_{E,l}^{-2})\leq t_k,\ \forall k,\ \forall l, \quad (67c)$$
$$\bar{t}_{k,l}\leq\boldsymbol{\phi}_{\imath(l)}^H\tilde{\mathbf{P}}_{k,l}\boldsymbol{\phi}_{\imath(l)}+2\mathrm{Re}\{\tilde{\mathbf{p}}_{k,l}^H\boldsymbol{\phi}_{\imath(l)}\}+c_{11_{k,l}},\ \forall k,\ \forall l, \quad (67d)$$

The above problem is non-convex due to its constraints (67b) and (67d). To tackle (P9), we first adopt MM method to convexify (67d) via linearization and then solve the following problem

$$(\mathrm{P10}): \min_{\boldsymbol{\phi}_R,\boldsymbol{\phi}_T,\mathbf{t},\bar{\mathbf{T}}} \ \boldsymbol{\phi}_R^H\mathbf{P}_R\boldsymbol{\phi}_R+2\mathrm{Re}\{\mathbf{p}_R^H\boldsymbol{\phi}_R\}$$
$$+\boldsymbol{\phi}_T^H\mathbf{P}_T\boldsymbol{\phi}_T+2\mathrm{Re}\{\mathbf{p}_T^H\boldsymbol{\phi}_T\}+\sum_{k=1}^{K}t_k+p \quad (68a)$$
$$\text{s.t. } (67\mathrm{b}),\ (67\mathrm{c}),$$
$$\bar{t}_{k,l}\leq 2\mathrm{Re}\{(\hat{\boldsymbol{\phi}}_{\imath(l)}^H\tilde{\mathbf{P}}_{k,l}+\tilde{\mathbf{p}}_{k,l}^H)\boldsymbol{\phi}_{\imath(l)}\}+\tilde{c}_{11_{k,l}},\ \forall k,\ \forall l, \quad (68b)$$

where $\hat{\boldsymbol{\phi}}_{\imath(l)}$ is any feasible solution obtained previously and $\tilde{c}_{11_{k,l}}=-(\hat{\boldsymbol{\phi}}_{\imath(l)}^H\tilde{\mathbf{P}}_{k,l}\hat{\boldsymbol{\phi}}_{\imath(l)})^*+c_{11_{k,l}}$.

Next, to tackle the difficult nonlinear equality constraint

This article has been accepted for publication in IEEE Transactions on Communications. This is the author's version which has not been fully edited and content may change prior to final publication. Citation information: DOI 10.1109/TCOMM.2023.3250454

(67b), we resort to the PDD framework [44]. We introduce auxiliary variables $\boldsymbol{\psi}_\imath$ and rewrite the problem (P10) as follows

$$
\begin{aligned}
(\text{P11}):\ &\min_{\boldsymbol{\phi}_R,\boldsymbol{\phi}_T,\boldsymbol{\psi}_R,\boldsymbol{\psi}_T,\mathbf{t},\bar{\mathbf{T}}}\ \boldsymbol{\phi}_R^H\mathbf{P}_R\boldsymbol{\phi}_R+2\mathrm{Re}\{\mathbf{p}_R^H\boldsymbol{\phi}_R\}\\
&\quad+\boldsymbol{\phi}_T^H\mathbf{P}_T\boldsymbol{\phi}_T+2\mathrm{Re}\{\mathbf{p}_T^H\boldsymbol{\phi}_T\}+\sum\nolimits_{k=1}^{K}t_k+c_9 \quad (69\text{a})\\
&\text{s.t. } (67\text{c}),\ (68\text{b}),\\
&\quad \boldsymbol{\phi}_\imath=\boldsymbol{\psi}_\imath,\ \imath\in\{R,T\}, \quad (69\text{b})\\
&\quad |\boldsymbol{\psi}_{\imath,m}|=1,\ \imath\in\{R,T\},\ \forall m, \quad (69\text{c})\\
&\quad |\boldsymbol{\phi}_{\imath,m}|\le 1,\ \imath\in\{R,T\},\ \forall m. \quad (69\text{d})
\end{aligned}
$$

Via penalizing the equality constraint (69b), we obatin the augmented Lagrangian problem of (P11) as follows

$$
\begin{aligned}
(\text{P12}):\ &\min_{\boldsymbol{\phi}_R,\boldsymbol{\phi}_T,\boldsymbol{\psi}_R,\boldsymbol{\psi}_T,\mathbf{t},\bar{\mathbf{T}}}\ \boldsymbol{\phi}_R^H\mathbf{P}_R\boldsymbol{\phi}_R+2\mathrm{Re}\{\mathbf{p}_R^H\boldsymbol{\phi}_R\}\\
&\quad+\boldsymbol{\phi}_T^H\mathbf{P}_T\boldsymbol{\phi}_T+2\mathrm{Re}\{\mathbf{p}_T^H\boldsymbol{\phi}_T\}+\sum\nolimits_{k=1}^{K}t_k+c_9\\
&\quad+\frac{1}{2\rho}\|\boldsymbol{\phi}_R-\boldsymbol{\psi}_R\|_2^2+\mathrm{Re}\{\boldsymbol{\lambda}_R^H(\boldsymbol{\phi}_R-\boldsymbol{\psi}_R)\}\\
&\quad+\frac{1}{2\rho}\|\boldsymbol{\phi}_T-\boldsymbol{\psi}_T\|_2^2+\mathrm{Re}\{\boldsymbol{\lambda}_T^H(\boldsymbol{\phi}_T-\boldsymbol{\psi}_T)\} \quad (70\text{a})\\
&\text{s.t. } (67\text{c}),\ (68\text{b}),\ (69\text{c}),\ (69\text{d}).
\end{aligned}
$$

According to [44], the PDD method is a two-layer iterative procedure, with its inner layer alternatively updating ($\boldsymbol{\phi}_R$, $\boldsymbol{\phi}_T$, $\mathbf{t}$, $\bar{\mathbf{T}}$) and ($\boldsymbol{\psi}_R$, $\boldsymbol{\psi}_T$) in a block coordinate descent (BCD) manner and the outer layer selectively updating the penalty coefficient ρ or the dual variables $\boldsymbol{\lambda}_\imath$, $\imath\in\{R,T\}$. The PDD procedure will be specified in the following.

As explained above, the PDD's inner layer in solving (P12) is a 2-block coordinate descent procedure. Specifically, when $(\boldsymbol{\psi}_R,\boldsymbol{\psi}_T)$ is fixed, the augmented Lagrangian problem is reduced to solving

$$
\begin{aligned}
(\text{P13}):\ &\min_{\boldsymbol{\phi}_R,\boldsymbol{\phi}_T,\mathbf{t},\bar{\mathbf{T}}}\ \boldsymbol{\phi}_R^H\mathbf{P}_R\boldsymbol{\phi}_R+2\mathrm{Re}\{\mathbf{p}_R^H\boldsymbol{\phi}_R\}\\
&\quad+\boldsymbol{\phi}_T^H\mathbf{P}_T\boldsymbol{\phi}_T+2\mathrm{Re}\{\mathbf{p}_T^H\boldsymbol{\phi}_T\}+\sum\nolimits_{k=1}^{K}t_k+c_9\\
&\quad+\frac{1}{2\rho}\|\boldsymbol{\phi}_R-\boldsymbol{\psi}_R\|_2^2+\mathrm{Re}\{\boldsymbol{\lambda}_R^H(\boldsymbol{\phi}_R-\boldsymbol{\psi}_R)\}\\
&\quad+\frac{1}{2\rho}\|\boldsymbol{\phi}_T-\boldsymbol{\psi}_T\|_2^2+\mathrm{Re}\{\boldsymbol{\lambda}_T^H(\boldsymbol{\phi}_T-\boldsymbol{\psi}_T)\} \quad (71\text{a})\\
&\text{s.t. } (67\text{c}),\ (68\text{b}),\ (69\text{d}),
\end{aligned}
$$

which is convex and can be numerically solved.

When $(\boldsymbol{\phi}_R,\boldsymbol{\phi}_T,\mathbf{t},\bar{\mathbf{T}})$ are fixed, the auxiliary variables $(\boldsymbol{\psi}_R,\boldsymbol{\psi}_T)$ are updated by solving the following problem

$$
\begin{aligned}
(\text{P14}):\ &\min_{\boldsymbol{\psi}_\mathbf{R},\boldsymbol{\psi}_\mathbf{R}}\ \frac{1}{2\rho}\|\boldsymbol{\phi}_R-\boldsymbol{\psi}_R\|_2^2+\mathrm{Re}\{\boldsymbol{\lambda}_R^H(\boldsymbol{\phi}_R-\boldsymbol{\psi}_R)\}\\
&\quad+\frac{1}{2\rho}\|\boldsymbol{\phi}_T-\boldsymbol{\psi}_T\|_2^2+\mathrm{Re}\{\boldsymbol{\lambda}_T^H(\boldsymbol{\phi}_T-\boldsymbol{\psi}_T)\} \quad (72\text{a})\\
&\text{s.t. } |\boldsymbol{\psi}_{R,m}|=1,\ \forall m\in\mathcal{M}, \quad (72\text{b})\\
&\quad\ |\boldsymbol{\psi}_{T,m}|=1,\ \forall m\in\mathcal{M}. \quad (72\text{c})
\end{aligned}
$$

Since $\boldsymbol{\psi}_\imath$ have unit modulus entries, the quadratic term with respect to $\boldsymbol{\psi}_\imath$ in the objective function (72a) are constant, i.e., $\frac{1}{2\rho}\|\boldsymbol{\psi}_R\|_2^2=\frac{M}{2\rho}$ and $\frac{1}{2\rho}\|\boldsymbol{\psi}_T\|_2^2=\frac{M}{2\rho}$. Therefore, the problem (P14) can be equivalently written as

$$
\begin{aligned}
(\text{P15}):\ &\max_{|\boldsymbol{\psi}_R|=\mathbf{1}_M,|\boldsymbol{\psi}_T|=\mathbf{1}_M}\ \mathrm{Re}\{(\boldsymbol{\phi}_R+\rho\boldsymbol{\lambda}_R)^H\boldsymbol{\psi}_R\}\\
&\quad+\mathrm{Re}\{(\boldsymbol{\phi}_T+\rho\boldsymbol{\lambda}_T)^H\boldsymbol{\psi}_T\}. \quad (73)
\end{aligned}
$$

Note that the maximum of (73) can be achieved when the phases of the elements of $\boldsymbol{\psi}_\imath$ are all aligned with those of $(\rho^{-1}\boldsymbol{\phi}_\imath+\boldsymbol{\lambda}_\imath)$, that are

$$\boldsymbol{\psi}_R^\star=\exp\big(j\cdot\angle(\boldsymbol{\phi}_R+\rho\boldsymbol{\lambda}_R)\big), \quad (74)$$

$$\boldsymbol{\psi}_T^\star=\exp\big(j\cdot\angle(\boldsymbol{\phi}_T+\rho\boldsymbol{\lambda}_T)\big). \quad (75)$$

Since the inner layer of PDD is a BCD procedure, its objective iterates monotonically converge. Once the convergence is achieved, the outer layer will conduct one of the following two operations

1) if the equalities $\boldsymbol{\phi}_R=\boldsymbol{\psi}_R$ and $\boldsymbol{\phi}_T=\boldsymbol{\psi}_T$ approximately hold, the dual variable $\boldsymbol{\lambda}_\imath$ will be updated in a gradient ascent manner, which is given by
$$\boldsymbol{\lambda}_\imath:=\boldsymbol{\lambda}_\imath+\rho^{-1}(\boldsymbol{\phi}_\imath-\boldsymbol{\psi}_\imath),\ \imath\in\{R,T\}; \quad (76)$$
2) otherwise, i.e., the equality constraints $\boldsymbol{\phi}_R=\boldsymbol{\psi}_R$ and/or $\boldsymbol{\phi}_T=\boldsymbol{\psi}_T$ are far from "being true", the outer layer will choose to increase the penalty parameter ρ^{-1}, which will force the equalities $\boldsymbol{\phi}_R=\boldsymbol{\psi}_R$ and $\boldsymbol{\phi}_T=\boldsymbol{\psi}_T$ to be better satisfied in the subsequent iterations, i.e.,
$$\rho^{-1}:=c^{-1}\cdot\rho^{-1}, \quad (77)$$
where c is a predetermined constant which is in the range of $(0,1)$ and typically chosen in the range of [0.8, 0.9].

The PDD-based method is summarized in Algorithm 1. The overall algorithm to solve (P2) is specified in Algorithm 2.

Algorithm 1 PDD Method to Solve (P10)

initialize $\boldsymbol{\phi}_\imath^{(0)}$, $\boldsymbol{\psi}_\imath^{(0)}$, $\boldsymbol{\lambda}_\imath^{(0)}$, $\rho^{(0)}$, $k=1$ and $\imath\in\{R,T\}$;
repeat
  set $\boldsymbol{\phi}_\imath^{(k-1,0)}:=\boldsymbol{\phi}_\imath^{(k-1)}$, $\boldsymbol{\psi}_\imath^{(k-1,0)}:=\boldsymbol{\psi}_\imath^{(k-1)}$, $t=0$;
  repeat
    update $\boldsymbol{\phi}_R^{(k-1,t+1)}$ and $\boldsymbol{\phi}_T^{(k-1,t+1)}$ by solving (P12);
    update $\boldsymbol{\psi}_R^{(k-1,t+1)}$ by (74);
    update $\boldsymbol{\psi}_T^{(k-1,t+1)}$ by (75);
    $t++$;
  until *convergence*
  set $\boldsymbol{\phi}_\imath^{(k)}:=\boldsymbol{\phi}^{(k-1,\infty)}$, $\boldsymbol{\psi}_\imath^{(k)}:=\boldsymbol{\psi}^{(k-1,\infty)}$;
  if $\|\boldsymbol{\phi}_R^{(k)}-\boldsymbol{\psi}_R^{(k)}\|_\infty\le\eta_k$ and $\|\boldsymbol{\phi}_T^{(k)}-\boldsymbol{\psi}_T^{(k)}\|_\infty\le\eta_k$ **then**
    $\boldsymbol{\lambda}_\imath^{(k+1)}:=\boldsymbol{\lambda}_\imath^{(k)}+\dfrac{1}{\rho^{(k)}}(\boldsymbol{\phi}_\imath^{(k)}-\boldsymbol{\psi}_\imath^{(k)})$, $\rho^{(k+1)}:=\rho^{(k)}$;
  else
    $\boldsymbol{\lambda}_\imath^{(k+1)}:=\boldsymbol{\lambda}_\imath^{(k)}$, $1/\rho^{(k+1)}:=1/(c\cdot\rho^{(k)})$;
  end if
  $k++$;
until $\|\boldsymbol{\phi}_R^{(k)}-\boldsymbol{\psi}_R^{(k)}\|_2$ and $\|\boldsymbol{\phi}_T^{(k)}-\boldsymbol{\psi}_T^{(k)}\|_2$ are sufficiently small simultaneously

Algorithm 2 Overall Algorithm to Solve (P2)

initialize $i = 0$;
randomly generate feasible $\{\mathbf{f}_k^{(0)}\}$, $\boldsymbol{\alpha}^{(0)}$, $\boldsymbol{\varsigma}^{(0)}$, $\boldsymbol{\phi}_\imath^{(0)}$ and $\imath \in \{R, T\}$;
repeat
  update $\boldsymbol{\beta}$, $\boldsymbol{\Omega}_E$ and $\boldsymbol{\omega}_B$ by (26), (27) and (28), respectively;
  update $\{\mathbf{f}_k^{(i+1)}\}$ by solving (P4);
  update $\boldsymbol{\alpha}^{(i+1)}$ by solving (P5);
  update $\boldsymbol{\varsigma}^{(i+1)}$ by solving (P8);
  update $\boldsymbol{\phi}_\imath^{(i+1)}$ by invoking Alg.1;
  $i++$;
until *convergence*

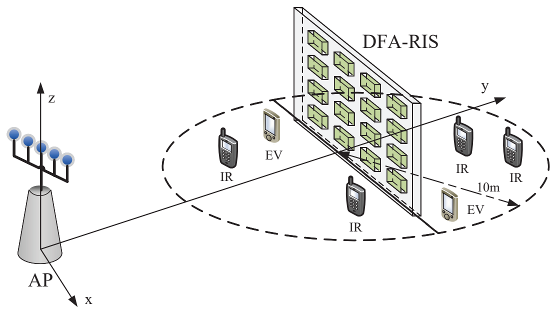

Fig. 3. The experiment scenario model.

G. Complexity

In this subsection, We will discuss the complexity of our proposed algorithms. According to the complexity analysis in [45], in the each iteration, the complexity of solving SOCP problems (P4), (P6) and (P8) are $\mathcal{O}((M + 2KL)KN(2(KN)^2 + M + 2KL))$, $\mathcal{O}((KL)^{1.5}M^3)$ and $\mathcal{O}((KL)^{1.5}M^3)$, respectively. For the PDD-based algorithm, the complexity of solving (P10) is $\mathcal{O}(C_2C_3(KL)^{1.5}M^3)$, where C_2 and C_3 denote the iteration number of the outer and inner PDD loops, respectively. Therefore, the total computational complexity of Algorithm 2 is approximately given as $\mathcal{O}(C_1((M + 2KL)KN(2(KN)^2 + M + 2KL) + C_2C_3(KL)^{1.5}M^3))$ with C_1 represented as the number of iterations to solve problem (P2).

V. Numerical Results

In this section, we provide numerical results to assess the performance of our proposed algorithm. The setting of the experiment is shown in Fig. 3, where one AP assisted by a DFA-RIS is serving 4 valid IRs and there are 2 EVs in the vicinity. In the experiment, the AP and DFA-RIS are located at the 3D coordinates (0, 0, 4.5m) and (0, 100m, 2.5m), respectively. The DFA-RIS divides the whole 3D space into two halves. In each half space, 2 IRs and 1 EV are randomly located within a circle of radius of 10m centered at the DFA-RIS at an altitude of 1.5m. The large scale fading is modeled as $PL = C_0(d/d_0)^{-\alpha}$, where C_0 corresponds to the path loss of the reference distance $d_0 = 1$m, d is the propagation distance and α is the fading exponent. The AP-RIS link follows Rician fading channel model with a Rician factor of 5dB. Both the AP-IR/EV links and the RIS-IR/EV links are all set to be Rayleigh fading channels. The path loss exponents of AP-IR, AP-EV, AP-RIS, RIS-IR and RIS-EV are $\alpha_{AI} = \alpha_{AE} = 3.5$, $\alpha_{AR} = 3.1$, $\alpha_{RI} = \alpha_{RE} = 2.8$, respectively. In addition, the AP equips $N = 4$ antennas and the DFA-RIS consists of $M = 50$ active units. The transmit power for the AP and the DFA-RIS is set as 20dBm and 16dBm respectively. The elementwise power limit for DFA-RIS is 2mW. The noise levels for IRs/EVs and DFA-RIS are set as $\sigma_{B,k}^2 = \sigma_{E,l}^2 = -90$dBm [46] and $\sigma_v^2 = -70$dBm [47], respectively.

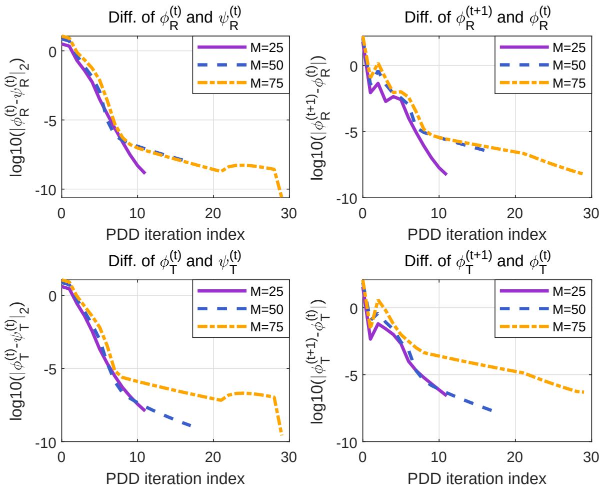

Fig. 4. Convergence of the proposed PDD algorithm.

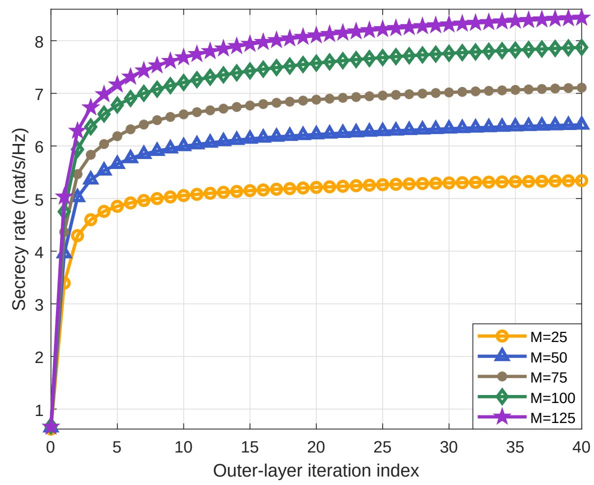

Fig. 5. Convergence of our proposed Alg. 2.

Fig. 4 investigates the converge performance of our proposed PDD algorithm to update phase shifts. In Fig. 4, we plot the difference between $\boldsymbol{\phi}_\imath$ and $\boldsymbol{\psi}_\imath$, $\imath \in \{R, T\}$, along with the outer iterations in the left plot and the difference of $\boldsymbol{\phi}_\imath$, $\imath \in \{R, T\}$, in the right plot with various M. As reflected in Fig. 4, the variation in $\boldsymbol{\phi}_\imath$ and difference between $\boldsymbol{\phi}_\imath$ and $\boldsymbol{\psi}_\imath$ becomes negligible (below 10^{-5}) within 30 iterations and hence the PDD algorithm converges well.

In Fig. 5, we examine the convergence behaviours of the

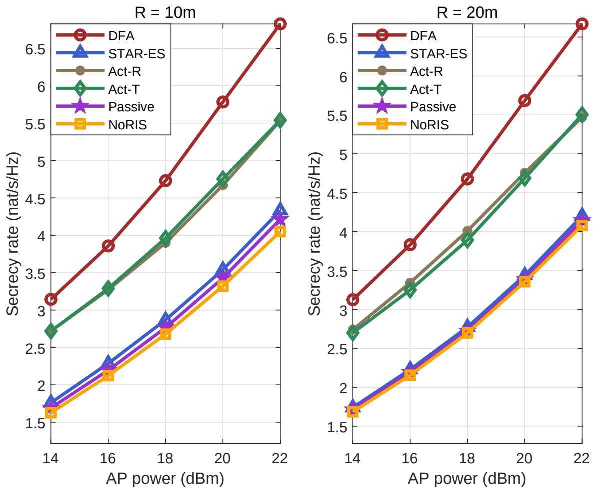

Fig. 6. The sum SR of different RIS architectures.

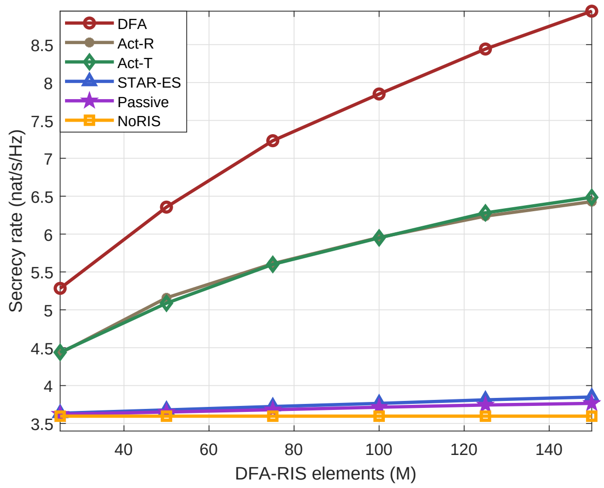

Fig. 7. The sum SR versus the number of RIS elements M.

overall solution Alg. 2. For each specific setting of M, the obtained SR iterates are illustrated in plot. As reflected in Fig. 5, our proposed solution yields monotonic improvement in SR. Generally, most of the beamforming gain can be achieved among the very first several iterations.

In Fig. 6, we compare DFA-RIS' performance in security enhancement with other cutting-the-edge RIS architectures, including

i) *Act-R*: This scheme corresponds to the single-faced active RIS architecture, as proposed in [7] and [8]. The letter 'R' means that the RIS' orientation is faced towards the reflective IRs and EVs. In this test, the transmissive IRs/EVs on the other side of the RIS will not receive signals from RIS

ii) *Act-T*: Similar as above, this scheme also considers the single-faced active RIS. As opposed to "Act-R", the orientation of active-RIS is faced towards the transmissive IRs/EVs in this case;

iii) *STAR-ES*: This scheme corresponds to the simultaneously transmitting and reflecting (STAR)-RIS technique operating in energy splitting (ES) mode, which was originally proposed in [10]. The energy splitting ratio between the transmissive and reflective signals is tunable within the range $[0, 1]$. Note the STAR-ES is passive RIS and hence its outgoing signal's power will not be enlarged;

iv) *Passive*: The conventional single-faced purely passive RIS proposed by the seminal papers [2]-[3] is utilized. The incoming signal is reflected with its phase being shifted;

v) No RIS is deployed in the system. This test case serves as a benchmark for comparison.

In addition, to make fair comparison, the AP's transmit power in the last three aforementioned scenarios is equal to the sum of the AP's and the RIS' transmit power of the active type RIS schemes. Specifically, when the supply power of AP in DFA-RIS scheme is only about 40% compared with the passive type RIS schemes, the DFA-RIS still can achieve the approximate level of secure communication. As shown in Fig.

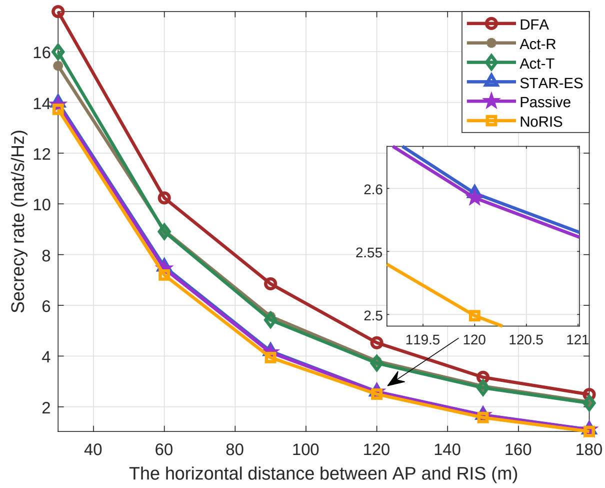

Fig. 8. The sum SR versus the horizontal distance between AP and RIS.

6, the obtained SR is increasing with the growing total transmit power. Fig. 6 clearly shows that the passive type RIS schemes yield limited SR improvement due to the severe double fading effect. Besides, the DFA-RIS significantly outperforms the single-faced RIS due to its full-space coverage.

Fig. 7 illustrates the impact of the number of RIS elements. Obviously, increasing the number of elements can improve beamforming gain for all RIS architectures. However, the SR's growing slope along with M associated with the passive-type RIS architectures is much lower that those of the active-type counterparts. This is, again, due to the severe double fading effect experienced by the pure passive RIS devices.

In Fig. 8, we examine the impact of the AP-RIS distance on the SR obtained by different RIS architectures. In our test, the distance between the AP and the RIS varies from 30m to 180m. As reflected by Fig. 8, within the wide range of AP-RIS distance that is tested, the DFA-RIS boosts the system's SR more significantly compared to all other competing schemes.

Fig. 9 investigates the impact of the number of AP's anten-

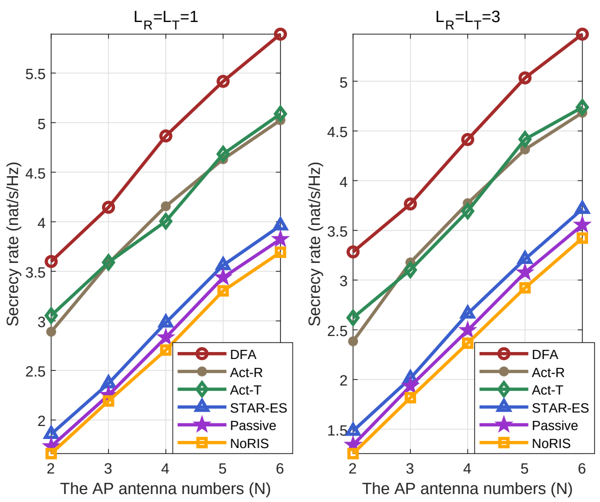

Fig. 9. The sum SR versus the number of AP antennas.

nas on the SR. It can be easily observed that a larger number of the AP antenna leads to a higher achievable SR in all schemes, and our proposed algorithm significantly outperforms other schemes. Besides, when $L_R = L_T = 3$, all schemes yield lower sum SR than the $L_R = L_T = 1$ case.

VI. Conclusions

This paper proposes a novel DFA-RIS architecture, which can effectively compensate the severe fading loss and achieve full-space coverage simultaneously. We exploit it to enhance the communication security. The proposed DFA-RIS beamforming design problem provides a unifying solution for other emerging RIS architectures and is highly challenging. Combining the MM and PDD methods, we develop an iterative solution that utilizes convex optimization techniques. Numerical results verify that the novel DFA-RIS can significantly outperform other state-of-the-art RIS architectures.

References

[1] C. Pan *et al.*, "An overview of signal processing techniques for RIS/IRS-aided wireless systems," *IEEE J. Sel. Topics Signal Process.*, vol. 16, no. 5, pp. 883-917, Aug. 2022.

[2] Q. Wu and R. Zhang, "Towards smart and reconfigurable rnvironment: Intelligent reflecting surface aided wireless network," *IEEE Commun. Mag.*, vol. 58, no. 1, pp. 106-112, Jan. 2020.

[3] Q. Wu, S. Zhang, B. Zheng, C. You, and R. Zhang, "Intelligent reflecting surface-aided wireless communications: A tutorial," *IEEE Trans. Commun.*, vol. 69, no. 5, pp. 3313-3351, May 2021.

[4] E. Björnson, Ö. Özdogan, and E. G. Larsson, "Intelligent reflecting surface versus decode-and-forward: How large surfaces are needed to beat relaying?" *IEEE Wireless Commun. Lett.*, vol. 9, no. 2, pp. 244-248, Feb. 2020.

[5] M. Najafi, V. Jamali, R. Schober, and H. V. Poor, "Physics-based modeling and scalable optimization of large intelligent reflecting surfaces," *IEEE Trans. Commun.*, vol. 69, no. 4, pp. 2673-2691, Apr. 2021.

[6] E. Basar and H. V. Poor, "Present and future of reconfigurable intelligent surface-empowered communications," *IEEE Signal Process. Mag.*, vol. 38, no. 6, pp. 146-152, Nov. 2021.

[7] Z. Zhang *et al.*, "Active RIS vs. passive RIS: Which will prevail in 6G?," *IEEE Trans. Commun.*, early access, December 23, 2022, doi: 10.1109/TCOMM.2022.3231893.

[8] R. Long, Y.-C. Liang, Y. Pei, and E. G. Larsson, "Active reconfigurable intelligent surface aided wireless communications," *IEEE Trans. Wireless Commun.*, vol. 20, no. 8, pp. 4962-4975, Mar. 2021.

[9] X. Xie, C. He, F. Gao, Z. Han, and Z. J. Wang, "Joint precoding for active intelligent transmitting surface empowered outdoor-to-indoor communication in mmWave cellular networks", Jun. 2022. [Online]. Available: https://arxiv.org/abs/2206.13801

[10] S. Zhang, H. Zhang, B. Di, Y. Tan, Z. Han, and L. Song, "Beyond intelligent reflecting surfaces: Reflective-transmissive metasurface aided communications for full-dimensional coverage extension," *IEEE Trans. Veh. Technol.*, vol. 69, no. 11, pp. 13905-13909, Nov. 2020.

[11] Y. Liu *et al.*, "STAR: Simultaneous transmission and reflection for 360° coverage by intelligent surfaces," *IEEE Wireless Commun.*, vol. 28, no. 6, pp. 102-109, Dec. 2021.

[12] H. Shen, W. Xu, S. Gong, Z. He, and C. Zhao, "Secrecy rate maximization for intelligent reflecting surface assisted multi-antenna communications," *IEEE Commun. Lett.*, vol. 23, no. 9, pp. 1488-1492, Sept. 2019.

[13] H. Niu, Z. Chu, F. Zhou, Z. Zhu, M. Zhang, and K.-K. Wong, "Weighted sum secrecy rate maximization using intelligent reflecting surface," *IEEE Trans. Commun.*, vol. 69, no. 9, pp. 6170-6184, Sept. 2021.

[14] X. Yu, D. Xu, Y. Sun, D. W. K. Ng, and R. Schober, "Robust and secure wireless communications via intelligent reflecting surfaces," *IEEE J. Sel. Areas Commun.*, vol. 38, no. 11, pp. 2637-2652, Nov. 2020.

[15] S. Hu, Z. Wei, Y. Cai, C. Liu, D. W. K. Ng, and J. Yuan, "Robust and secure sum-rate maximization for multiuser MISO downlink systems with self-sustainable IRS," *IEEE Trans. Commun.*, vol. 69, no. 10, pp. 7032-7049, Oct. 2021.

[16] L. Lv, Q. Wu, Z. Li, Z. Ding, N. Al-Dhahir, and J. Chen, "Covert communication in intelligent reflecting surface-assisted NOMA systems: Design, analysis, and optimization," *IEEE Trans. Wireless Commun.*, vol. 21, no. 3, pp. 1735-1750, Mar. 2022.

[17] L. Dong, H.-M. Wang, and J. Bai, "Active reconfigurable intelligent surface aided secure transmission," *IEEE Trans. Veh. Technol.*, vol. 71, no. 2, pp. 2181-2186, Feb. 2022.

[18] W. Lv, J. Bai, Q. Yan, and H. -M. Wang, "RIS-assisted green secure communications: Active RIS or passive RIS?," *IEEE Wireless Commun. Lett.*, early access, November 24, 2022, doi: doi: 10.1109/LWC.2022.3221609.

[19] S. Hu, D. W. K. Ng, and J. Yuan, "Secure communication in multifunctional active intelligent reflection surface-assisted systems," May 2022. [Online]. Available: https://arxiv.org/abs/2205.02512

[20] H. Niu *et al.*, "Joint beamforming design for secure RIS-assisted IoT networks," *IEEE Internet Things J.*, early access, September 27, 2022, doi: 10.1109/JIOT.2022.3210115.

[21] H. Niu, Z. Chu, F. Zhou, and Z. Zhu, "Simultaneous transmission and reflection reconfigurable intelligent surface assisted secrecy MISO networks," *IEEE Commun. Lett.*, vol. 25, no. 11, pp. 3498-3502, Nov. 2021.

[22] Y. Han, N. Li, Y. Liu, T. Zhang, and X. Tao, "Artificial noise aided secure NOMA communications in STAR-RIS networks," *IEEE Wireless Commun. Lett.*, vol. 11, no. 6, pp. 1191-1195, Jun. 2022.

[23] Z. Zhang, Z. Wang, Y. Liu, B. He, L. Lv, and J. Chen, "Security enhancement for coupled phase-shift STAR-RIS networks," Aug. 2022. [Online]. Available: https://arxiv.org/abs/2208.10382

[24] W. Wang, W. Ni, H. Tian, Z. Yang, C. Huang, and K. -K. Wong, "Safeguarding NOMA networks via reconfigurable dual-functional surface under imperfect CSI," *IEEE J. Sel. Topics Signal Process.*, vol. 16, no. 5, pp. 950-966, Aug. 2022.

[25] W. Wang, W. Ni, H. Tian, and L. Song, "Intelligent omni-surface enhanced aerial secure offloading," *IEEE Trans. Veh. Technol.*, vol. 71, no. 5, pp. 5007-5022, May 2022.

[26] K. K. Kishor and S. V. Hum, "An amplifying reconfigurable reflectarray antenna," *IEEE Trans. Ant. Propag.*, vol. 60, no. 1, pp. 197-205, 2012.

[27] F. Farzami, S. Khaledian, B. Smida, and D. Erricolo, "Reconfigurable dual-band bidirectional reflection amplifier with applications in Van Atta array," *IEEE Trans. Microw. Theory Techn.*, vol. 65, no. 11, pp. 4198-4207, Nov. 2017.

[28] S. Khaledian, F. Farzami, D. Erricolo, and B. Smida, "A full-duplex bidirectional amplifier with low DC power consumption using tunnel diodes," *IEEE Microw. Wireless Compon. Lett.*, vol. 27, no. 12, pp. 1125-1127, Dec. 2017.

[29] N. Landsberg and E. Socher, "Design and measurements of 100 GHz reflectarray and transmitarray active antenna cells," *IEEE Trans. Ant. Propag.*, vol. 65, no. 12, pp. 6986-6997, Dec. 2017.

[30] N. Landsberg and E. Socher, "A Low-Power 28-nm CMOS FD-SOI reflection amplifier for an active F-band reflectarray," *IEEE Trans. Microw. Theory Techn.*, vol. 65, no. 10, pp. 3910-3921, Oct. 2017.

[31] Y. Wu, L. Jiao, B. Zhang, M. Li, W. Wang, and Y. Liu, "A new coupler structure with phase-controlled power divisions of extremely-wide tunable ranges and arbitrary phase differences," *IEEE Access*, vol. 6, pp. 10121-10130, 2018.

[32] H. N. Chu and T.-G. Ma, "Tunable directional coupler with very wide tuning range of power division ratio," *IEEE Microw. Wireless Comp. Lett.*, vol. 29, no. 10, pp. 652-654, Oct. 2019.

[33] H. N. Chu and T.-G. Ma, "A coupler with wide power division ratio tuning range and flexible coupling direction," *IEEE Microw. Wireless Comp. Lett.*, vol. 31, no. 2, pp. 121-124, Feb. 2021.

[34] H. Peng, P. Lei, H. Yang, S. Zhao, and X. Ding, "Π-type reconfigurable coupler based on a complementary tunable method," *J. Electr. Waves App.*, 2021.

[35] S. Ilyas, N. Shoaib, S. Nikolaou, and H. M. Cheema, "A wideband tunable power divider for SWIPT systems," *IEEE Access*, vol. 8, pp. 30675-30681, 2020.

[36] T. Xie *et al.*, "2-way power divider with wide tunable power ratio range for weighted-polarization MIMO antenna in BAN radios at 2.45 GHz," *IEEE Ant. Wireless Propag. Lett.*, vol. 21, no. 7, pp. 1333-1337, Jul. 2022.

[37] L. Wu *et al.*, "A wideband amplifying reconfigurable intelligent surface," *IEEE Trans. Antennas Propag.*, vol. 70, no. 11, pp. 10623-10631, Nov. 2022.

[38] Y. Xiao, F. Lin, H. Ma, X. Tan, and H. Sun, "A planar balanced power divider with tunable power-dividing ratio," *IEEE Trans. Microw. Theory Techn.*, vol. 65, no. 12, pp. 4871-4882, Dec. 2017.

[39] F. Shu, X. Wu, J. Hu, J. Li, R. Chen, and J. Wang, "Secure and precise wireless transmission for random-subcarrier-selection-based directional modulation transmit antenna array," *IEEE J. Sel. Areas Commun.*, vol. 36, no. 4, pp. 890-904, Apr. 2018.

[40] E. Choi, M. Oh, J. Choi, J. Park, N. Lee, and N. Al-Dhahir, "Joint precoding and artificial noise design for MU-MIMO wiretap channels," *IEEE Transa. Commun.*, early access, December 07, 2022, doi: 10.1109/TCOMM.2022.3227284.

[41] Q. Shi, M. Razaviyayn, Z. -Q. Luo, and C. He, "An iteratively weighted MMSE approach to distributed sum-utility maximization for a MIMO interfering broadcast channel," *IEEE Trans. Signal Process.*, vol. 59, no. 9, pp. 4331-4340, Sept. 2011.

[42] Y. Sun, P. Babu, and D. P. Palomar, "Majorization-minimization algorithms in signal processing, communications, and machine learning," *IEEE Trans. Signal Process.*, vol. 65, no. 3, pp. 794-816, Feb. 2017.

[43] M. Grant and S. Boyd, *CVX: Matlab software for disciplined convex programming*, version 2.1, http://cvxr.com/cvx, Mar. 2014.

[44] Q. Shi and M. Hong, "Penalty dual decomposition method for nonsmooth nonconvex optimization-part i: Algorithms and convergence analysis," *IEEE Trans. Signal Process.*, vol. 68, pp. 4108-4122, Jun. 2020.

[45] A. Ben-Tal and A. Nemirovski, "Lectures on Modern Convex Optimization, Analysis, Algorithms, and Engineering Applications." *Society for Industrial and Applied Mathematics (SIAM)*, 2001.

[46] P. Zeng, D. Qiao, Q. Wu, and Y. Wu, "Throughput maximization for active intelligent reflecting surface-aided wireless powered communications," *IEEE Wireless Commun. Lett.*, vol. 11, no. 5, pp. 992-996, May 2022.

[47] C. You and R. Zhang, "Wireless communication aided by intelligent reflecting surface: Active or passive?," *IEEE Wireless Commun. Lett.*, vol. 10, no. 12, pp. 2659-2663, Dec. 2021.

Yuan Guo received the B.S. degree in Communication Engineering from Northeast Forestry University, China, in 2021. He is currently pursuing the M.S. degree with the School of Information and Communication Engineering, Dalian University of Technology (DUT), China. His current research interests include intelligent reflecting surfaces, physical layer security, and integrated sensing and communication.

Yang Liu received the Ph.D. degree in Electrical Engineering from Lehigh University, PA, USA, in 2016. Before that he received the B.E. and M.E. degrees in Electrical Engineering from Beijing University of Posts and Telecommunications (BUPT), Beijing, China, in 2007 and 2010, respectively. In 2016, He worked as a senior engineer in Marvell Semiconductor Ltd., Santa Clara, CA, USA. From 2016 to 2019, he worked as a research engineer in Huawei Technologies Co., Ltd., Shanghai, China. From Nov. 2019 to April 2020, he worked as a postdoctoral research fellow in Nanyang Technological University (NTU), Singapore. He is currently an associate professor in the School of Information and Communication Engineering, Dalian University of Technology, Dalian, China. His research interests include error correction coding, multi-antenna wireless communication systems, intelligent reflective surface and wireless sensor networks.

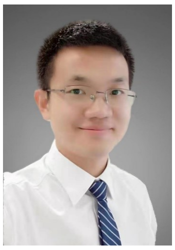

Qingqing Wu (S'13-M'16-SM'21) received the B.Eng. and the Ph.D. degrees in Electronic Engineering from South China University of Technology and Shanghai Jiao Tong University (SJTU) in 2012 and 2016, respectively. From 2016 to 2020, he was a Research Fellow in the Department of Electrical and Computer Engineering at National University of Singapore. His current research interest includes intelligent reflecting surface (IRS), unmanned aerial vehicle (UAV) communications, and MIMO transceiver design. He has coauthored more than 100 IEEE journal papers with 26 ESI highly cited papers and 8 ESI hot papers, which have received more than 15,000 Google citations. He was listed as the Clarivate ESI Highly Cited Researcher in 2022 and 2021, the Most Influential Scholar Award in AI-2000 by Aminer in 2021 and Worlds Top 2

He was the recipient of the IEEE Communications Society Asia Pacific Best Young Researcher Award and Outstanding Paper Award in 2022, the IEEE Communications Society Young Author Best Paper Award in 2021, the Outstanding Ph.D. Thesis Award of China Institute of Communications in 2017, the Outstanding Ph.D. Thesis Funding in SJTU in 2016, the IEEE ICCC Best Paper Award in 2021, and IEEE WCSP Best Paper Award in 2015. He was the Exemplary Editor of IEEE Communications Letters in 2019 and the Exemplary Reviewer of several IEEE journals. He serves as an Associate Editor for IEEE Transactions on Communications, IEEE Communications Letters, IEEE Wireless Communications Letters, IEEE Open Journal of Communications Society (OJ-COMS), and IEEE Open Journal of Vehicular Technology (OJVT). He is the Lead Guest Editor for IEEE Journal on Selected Areas in Communications on "UAV Communications in 5G and Beyond Networks", and the Guest Editor for IEEE OJVT on "6G Intelligent Communications" and IEEE OJ-COMS on Reconfigurable Intelligent Surface-Based Communications for 6G Wireless Networks". He is the workshop co-chair for IEEE ICC 2019-2022 workshop on Integrating UAVs into 5G and Beyond, and the workshop co-chair for IEEE GLOBECOM 2020 and ICC 2021 workshop on Reconfigurable Intelligent Surfaces for Wireless Communication for Beyond 5G. He serves as the Workshops and Symposia Officer of Reconfigurable Intelligent Surfaces Emerging Technology Initiative and Research Blog Officer of Aerial Communications Emerging Technology Initiative. He is the IEEE Communications Society Young Professional Chair in Asia Pacific Region.

Qingjiang Shi received his Ph.D. degree in electronic engineering from Shanghai Jiao Tong University, Shanghai, China, in 2011. From September 2009 to September 2010, he visited Prof. Z.-Q. (Tom) Luo's research group at the University of Minnesota, Twin Cities. In 2011, he worked as a Research Scientist at Bell Labs China. From 2012, He was with the School of Information and Science Technology at Zhejiang Sci-Tech University. From Feb. 2016 to Mar. 2017, he worked as a research fellow at Iowa State University, USA. From Mar. 2018, he is currently a full professor with the School of Software Engineering at Tongji University. He is also with the Shenzhen Research Institute of Big Data. His interests lie in algorithm design and analysis with applications in machine learning, signal processing and wireless networks. So far he has published more than 70 IEEE journals and filed about 30 national patents.

Dr. Shi was an Associate Editor for the IEEE TRANSACTIONS ON SIGNAL PROCESSING. He was the recipient of the Huawei Outstanding Technical Achievement Award in 2021, the Huawei Technical Cooperation Achievement Transformation Award (2nd Prize) in 2022, the Golden Medal at the 46th International Exhibition of Inventions of Geneva in 2018, the First Prize of Science and Technology Award from China Institute of Communications in 2017, the National Excellent Doctoral Dissertation Nomination Award in 2013, the Shanghai Excellent Doctorial Dissertation Award in 2012, and the Best Paper Award from the IEEE PIMRC'09 conference.

Yang Zhao (S'19) is currently working in Singapore Institute of Manufacturing Technology, Agency for Science, Technology & Research. She received her PhD degree in School of Computer Science and Engineering, Nanyang Technological University, Singapore. She received her master (2015) degree in Electrical Engineering from National University of Singapore. Her research interests include federated learning, blockchain, differential privacy, and 6G.